Solid Earth, 16, 619–640, 2025
https://doi.org/10.5194/se-16-619-2025


Solid Earth

# Evidence for multi-rifting in the Variscan–Alpine cycle transition: insights from the European western Southern Alps

**Emanuele Scaramuzzo**[1], **Franz A. Livio**[1], **Maria Giuditta Fellin**[2], **and Colin Maden**[2]

[1]Department of Science and High Technology, University of Insubria, via Valleggio 11, 22100 Como, Italy
[2]Department of Earth and Planetary Sciences, ETH Zürich, Sonneggstrasse 5, 8092 Zurich, Switzerland

**Correspondence:** Maria Giuditta Fellin (giuditta.fellin@eaps.ethz.ch)

Received: 15 April 2024 – Discussion started: 29 April 2024
Revised: 17 February 2025 – Accepted: 16 April 2025 – Published: 10 July 2025

**Abstract.** We investigate the transition between the Paleozoic Variscan cycle and the Mesozoic–Cenozoic Alpine supercontinent cycle, both of which have played a pivotal role in shaping the central European–Mediterranean plate architecture. Two main scenarios have been proposed so far for this transition: (i) a single, long-lasting, Permo-Triassic rifting event, culminating in the opening of the Alpine Tethys, or (ii) multiple, distinct rifting events, predating the onset of the Alpine cycle. Our study focuses on the European western Southern Alps (Varese area, N. Italy), where we document the tectonic events from the early Permian to the Middle Triassic. Through a combined tectono-stratigraphic and thermochronological analysis, we identify an initial early Permian rifting stage linked to magmatic activity, followed by early–middle Permian transcurrent tectonics. This phase is truncated by a middle Permian regional-scale erosional event that marks the cessation of this tectonic phase. Subsequently, during the Middle Triassic, a second phase initiated, which we interpret as the onset of the Alpine Tethys opening. This phase likely corresponds to an early stretching stage that predates the well-documented Late Triassic crustal-thinning phase. Based on our findings, we propose that the Middle Triassic stretching phase represents the first stage of the Alpine Tethys rifting, thereby challenging the hypothesis of a continuous Permo-Triassic long-lasting extension.

## 1 Introduction

The Paleozoic Variscan cycle and the successive Mesozoic–Cenozoic Alpine supercontinent cycle (sensu Wilson, 1968; Wilson et al., 2019, and references therein) have shaped the structural framework of the central European–Mediterranean plate (e.g. Stampfli and Kozur, 2006; Ballèvre et al., 2020; Elter et al., 2020; Molli et al., 2020). Due to the large hiatus in the geological record spanning from the latest Paleozoic to the earliest Mesozoic, the transition between the two cycles is open to different interpretations. As a remnant of the Variscan chain (Fig. 1a), the European Southern Alps stand as an ideal study area to unravel the geodynamic processes governing the transition between the two cycles. In this region, three main events took place during this transition.

Firstly, the deposition of an upper Carboniferous siliciclastic cover on the Variscan metamorphic basement was followed by early Permian crustal thinning and calc-alkaline magmatism throughout the former peri-Variscan chain (e.g. Stampfli, 1996, 2000; Ziegler and Stampfli, 2001; Stampfli and Kozur, 2006; Cassinis et al., 2012; Cassinis et al., 2018; Ballèvre et al., 2020; Molli et al., 2020). Then, a non-depositional, erosive phase cut through this succession all around the Mediterranean area during the early–middle Permian (e.g. Cassinis et al., 2012; Gretter et al., 2013; Cassinis et al., 2018, and references therein). The resulting erosive surface was later covered by discontinuous, upper–middle Permian to Lower Triassic continental to shallow water marine sediments followed by discontinuous platforms and intra-platform basins successions (e.g. Bernoulli, 2007; Gaetani, 2010, and references therein). Finally, crustal thinning started in the Late Triassic (e.g. Bertotti et al., 1993).

Two main scenarios have been postulated so far to explain how the transition between the Variscan and the Alpine cycles occurred: in the first scenario, the succession of events described above relates to a long-lasting, single-rifting event between the demise of the Variscan cycle in the late Car-

Published by Copernicus Publications on behalf of the European Geosciences Union.

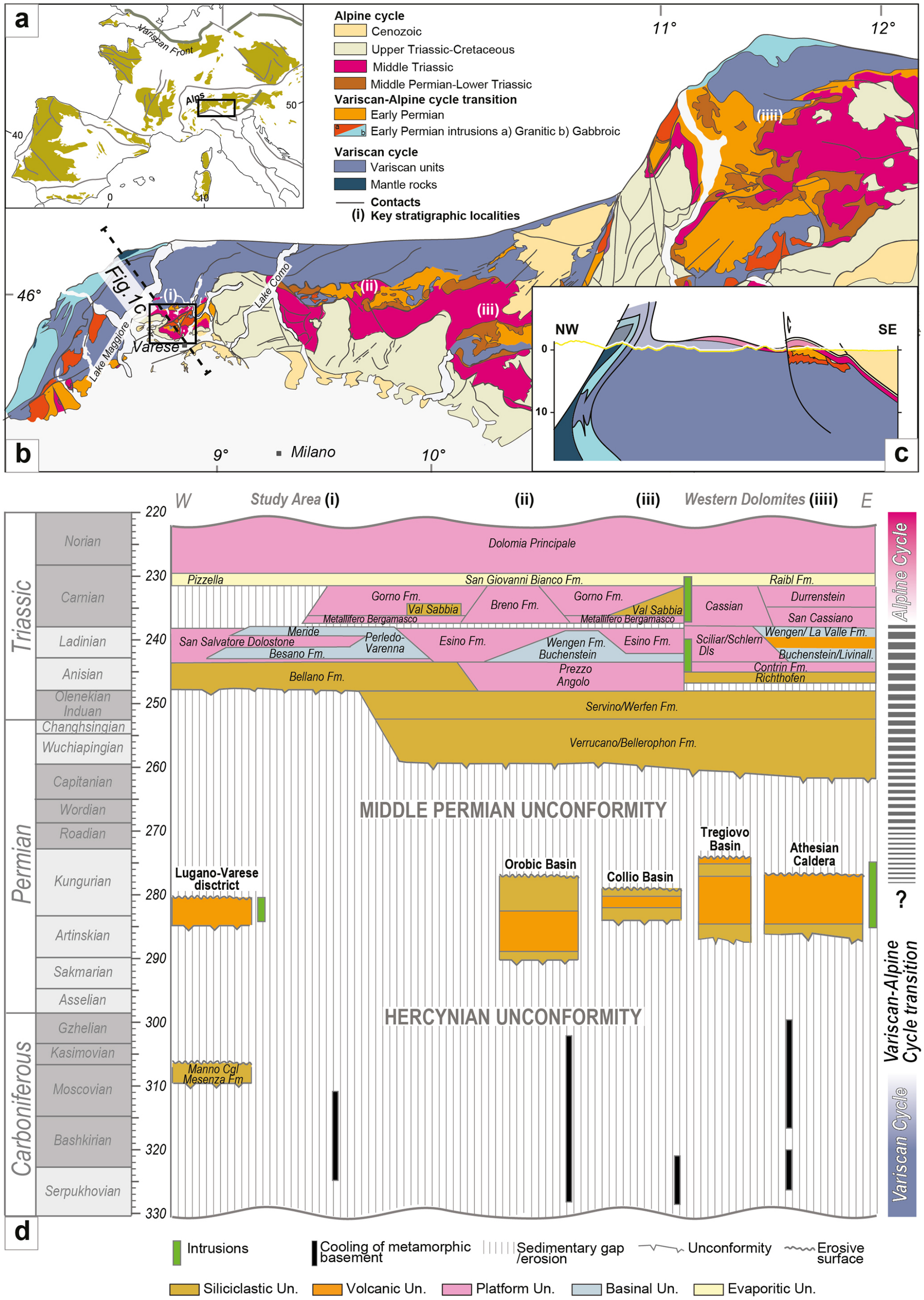


**Figure 1.** Regional geological setting and stratigraphy: **(a)** distribution of the Palaeozoic peri-Variscan terrain in the Mediterranean area (modified after Von Raumer et al., 2002), **(b)** simplified geological map of the Southern Alps modified after Bigi et al. (1990), **(c)** crustal-scale cross-section along the western sector of the Southern Alps (redrawn after Scaramuzzo et al., 2022) and **(d)** chronostratigraphic scheme of Carboniferous–Jurassic succession of the Southern Alps with the sequence subdivision adopted in this paper for the study area (redrawn after Schaltegger and Brack, 2007; Berra et al., 2009; Cassinis et al., 2012; Gretter et al., 2013; Beltrando et al., 2015; Cassinis et al., 2018).

boniferous and the onset of the Alpine one in the Late Triassic (e.g. Winterer and Bosellini, 1981; Siletto et al., 1993; Zanoni and Spalla, 2018; Roda et al., 2019). In the alternative scenario, successive and distinct rifting events (hereafter referred to as multi-rifting) intervened between the two cycles (e.g. Ziegler and Stampfli, 2001; Stampfli et al., 2000; Stampfli and Kozur, 2006, and references therein) and the break between the two cycles occurred at the end of the transition, in the Triassic. According to the single rifting model, the early Permian tectonic phase represents the onset of a single, long-lasting rifting event, under the same plate kinematic framework, culminating with the opening of the Alpine Tethys (e.g. Winterer and Bosellini, 1981; Siletto et al., 1993; Zanoni and Spalla, 2018; Roda et al., 2019). Conversely, according to the multi-rifting model, the Late Triassic opening of the Alpine Tethys was preceded by a series of aborted rifting events, taking place under diverse plate kinematic directions (e.g. Ziegler and Stampfli, 2001; Stampfli and Kozur, 2006, and references therein). Several models are concordant with the multi-rifting hypothesis, but each one proposes different mechanisms to explain the succession of distinct rifting events from the early Permian to the Middle Triassic. For instance, Muttoni et al. (2003, 2009) and Schaltegger and Brack (2007) concluded that multi-rifting reflects wrench tectonics related to the reconfiguration of Pangea from an Irving type (Pangea B) to a Wegener type (Pangea A). Alternatively, Malavieille et al. (1990) suggested that extension in the early Permian was caused by the orogenic collapse of the Variscan chain. Finally, the early Permian extension could reflect back-arc thinning triggered by the subduction of the Paleo-Tethys Ocean beneath the southeastern margin of the Pangea continent (Visonà, 1982; Lorenz and Nicholls, 1984; Stille and Buletti, 1987; Di Battistini et al., 1988; Finger and Steyrer, 1990, 1991; Bonin et al., 1993; Doglioni, 1995; Stampfli and Kozur, 2006).

A combined tectono-stratigraphic and low-temperature thermochronological approach on a sector of the former Variscan chain accreted within the western sector of the Southern Alpine chain here provides novel constraints on the Variscan–Alpine cycles transition. The pristine geological and thermochronological record of the study area shows that the Variscan–Alpine orogenic cycle changeover is marked by a main aborted rifting phase, separated by a transcurrent phase, thus supporting the multi-rifting interpretation.

## 2 Geological background

### 2.1 Regional tectonic framework

The Southern Alps stand as a remnant of the Variscan chain (Fig. 1a) that underwent rifting during the Mesozoic, ultimately transforming into the distant passive margin of the northern sector of the Africa Plate, e.g. Adria (e.g. Zingg et al., 1990; Bertotti et al., 1993; Handy et al., 1999; Ferrando et al., 2004; Bernoulli, 2007; Schaltegger and Brack, 2007). This belt is composed of Adria-derived units stacked along alpine south-verging thrusts, which accommodated reduced shortening in the west (Rosenberg and Kissling, 2013), locally reactivating inherited structures (Fig. 1b, c; e.g. Scaramuzzo et al., 2022). The fragments of the Variscan chain exposed in the Southern Alps are made up of an assemblage of several tectono-metamorphic units (e.g. Diella et al., 1992; Siletto et al., 1993; Boriani and Villa, 1997; Di Paola et al., 2001; Boriani et al., 2003; Spalla et al., 2006). In the study area, these units consist of amphibolitic facies, para- and ortho-gneisses, and schists (Serie dei Laghi Unit; e.g. Boriani et al., 1990; Handy et al., 1999; Fig. 3). These experienced peak metamorphism in the early Carboniferous (340–320 Ma) and cooled to moderate temperatures in the late Carboniferous (ca. 305 Ma), when they reached middle crustal depths, as documented by Rb–Sr age on white mica and biotite (Fig. 1d; Schaltegger and Brack, 2007, and references therein). The top of the Variscan basement is marked by a regional erosional surface, the Hercynian Unconformity (Handy et al., 1999). This is overlain locally by Middle Pennsylvanian (ca. 310 Ma) continental conglomerates (i.e. Manno Conglomerate and Mesenzana Fm., Fig. 1d; Jongmans and Ritter, 1960; Casati, 1978; Cassinis et al., 2012). During the early Permian (i.e. between 285 and 275 Ma), mafic to acid plutonic rocks with mantle melt involvement intruded the peri-Variscan metamorphic rocks at lower to upper crustal depths (Fig. 1d; Barth et al., 1994; Schaltegger and Brack, 2007; Cassinis et al., 2012; Berra et al., 2015; Karakas et al., 2019). This magmatic activity was accompanied by the deposition within caldera complexes of thick successions of volcanic products with calc-alkaline affinity together with clastic continental sediments (Collio, Orobic and Tregiovo basins and Athesian and Sesia Valley caldera; Fig. 1d; Bakos et al., 1990; Schaltegger and Brack 2007; Marocchi et al., 2008; Quick et al., 2009; Berra et al., 2015; Berra et al., 2016). In the study area, the lower Permian intrusive rocks consist of aplitic microgranites, granites, and quartz-bearing, NE–SW striking, micro-porphyric dikes, which altogether form a subvolcanic complex (i.e. Ganna Granitic Stock; Baggio and De Marco, 1960; Govi, 1960; Stille and Buletti, 1987; Bakos et al., 1990; Schaltegger and Brack, 2007). The emplacement of the Ganna Granitic complex occurred at $281.34 \pm 0.48$ Ma (Schaltegger and Brack, 2007), near the surface, at pressures most likely in the range of 0.5–0.75 kbar and certainly less than 2 kbar (Bakos et al., 1990), implying a maximum thickness of the units overlying the intrusive complex of 2–5 km. Tuffs, ignimbrites and andesitic to dacitic lavas with thin intercalations of clastic rocks of lower Permian age are extensively exposed in the study area (Baggio and De Marco, 1960; Govi, 1960; Stille and Buletti, 1987; Bakos et al., 1990; Schaltegger and Brack, 2007).

Across the Southern Alps, a middle Permian erosive surface (the "middle Permian Unconformity", hereafter; Fig. 1d) lies over the top of the exhumed composite metamorphic basement and the lower Permian succession, marking a depositional hiatus of ca. 15 to 20 million years (Fig. 1d; e.g. Bernoulli, 2007; Schaltegger and Brack, 2007; Gaetani, 2010; Cassinis et al., 2012; Gretter et al., 2013; Cassinis et al., 2018). At middle crustal levels, pervasive extensional deformation is recorded during the middle–late Permian by the metamorphic basement north of the Lake Como (Real et al., 2023). The middle Permian Unconformity is overlain by a diachronous sedimentary wedge consisting of continental siliciclastic deposits and minor coastal marine sediments, which spans the uppermost middle Permian to the Lower–Middle Triassic (Fig. 1d; i.e. Verrucano Fm. and Servino Fm.; e.g. Bernoulli, 2007; Gaetani, 2010; Cassinis et al., 2012; Cassinis et al., 2018). During the Anisian stage, mixed carbonate/fine siliciclastic deposits were deposited over an extensive area (e.g. Gaetani et al., 1998; Brack and Rieber, 1993; Bernoulli, 2007; Gaetani, 2010). In the study area, the Anisian siliciclastic deposits consist of micro-conglomerates with centimetric rounded quartz clasts dispersed in a red matrix and of thin-bedded siltstones and fine sandstones with plane-parallel or cross laminations (i.e. Bellano Fm; Fig. 1d; Stockar et al., 2013). At the middle–upper Anisian boundary, siliciclastic deposition ended throughout the Southern Alps, and substantial carbonate platform grew in proximal areas and alternated with intra-platform basins, which hosted anoxic sediments simultaneously with volcanic activity (Fig. 1d; e.g. Gaetani et al., 1998; Brack and Rieber, 1993; Bernoulli, 2007; Gaetani, 2010; Storck et al., 2019; De Min et al., 2020). During this stage, the local formations consist of dolomitic limestones that were deposited in reef and shallow-sea environments (Dolomia di San Salvatore) and that are laterally heteropic with intra-platform limestones and anoxic shales (Meride Limestones and Besano Shales; Fig. 1d; Bernoulli, 1964; Zorn, 1971; Furrer, 1995; Bernoulli, 2007; Stockar, 2010; Stockar et al., 2013; Renesto and Stockar, 2018). The end of the Carnian is marked across the Southern Alps by the deposition of terrigenous, evaporitic, and lesser carbonate sediments associated with sea-level fall together with the input of siliciclastic and volcanic detritus (Fig. 1d; i.e. Pizzella Marls, San Giovanni Bianco Fm., Raibl Fm.; e.g. Bernoulli, 2007; Gaetani, 2010). The late Anisian to early Carnian development and emersion of carbonate platform was simultaneous with a thermal event recorded by the basement rocks north of the Lake Como, which underwent static recrystallisation (Real et al., 2023). During the latest Carnian, the subsidence rate gradually decreased, and the volcanic activity ceased (e.g. Bernoulli, 2007; Gaetani, 2010). Subsidence resumed in the Norian and increased rapidly as crustal thinning progressed (e.g. Bertotti et al., 1993; Gaetani, 2010).

## 2.2 Thermochronological record

The thermochronologic record of the units accreted within the Southern Alpine chain (Fig. 2) spans the Carboniferous Period to the Miocene Epoch. Most commonly, the lowest-temperature (low-T) thermochronometric data, including fission-track and (U–Th)/He ages on apatite and zircon, record the thermal overprint related to the Mesozoic and Cenozoic events of the Alpine cycle (Giger, 1991; Martin et al., 1998; Bertotti et al., 1999; Zattin et al., 2006; Siegesmund et al., 2008; Zanchetta et al., 2011, 2015; Berger et al., 2012; Pomella et al., 2012; Reverman et al., 2012; Wolff et al., 2012; Beltrando et al., 2015; Heberer et al., 2016). Higher-temperature (high-T) thermochronometric systems, like Rb/Sr, K/Ar, and Ar/Ar, record also older events that locally date back to the end of the Variscan cycle during the Carboniferous (Fig. 2a, b; McDowell and Schmid, 1968; McDowell, 1970; Bertotti et al., 1999; Siegesmund et al., 2008; Zanchetta et al., 2011; Wolff et al., 2012). In the central sector of the Southern Alps area, near Lake Como, Jurassic to Early Cretaceous zircon fission-track ages (Fig. 2c) indicate continued cooling from rifting until the onset of Alpine convergence, whereas Late Triassic to Jurassic high-T thermochronometric ages (Rb/Sr and Ar/Ar) document altered thermal conditions before and at the onset of rifting (Bertotti et al., 1999). In the western sector of the Southern Alps, west of Lake Maggiore, apatite fission-track ages are all Eocene and younger, whereas fission-track and (U–Th)/He ages on zircon are Triassic to Miocene, and high-T thermochronometric ages (muscovite and biotite K/Ar; Fig. 2a, b) are Carboniferous to Jurassic (McDowell and Schmid, 1968; McDowell, 1970; Hurford, 1986; Siegesmund et al., 2008; Wolff et al., 2012). In the westernmost sector of the Southern Alps, bedrock and detrital zircon (U–Th)/He ages (Fig. 2d) record a protracted thermal history that starts in the Late Triassic in relation to crustal thinning and continues until the Cretaceous, resulting in wide and complex age distributions in both bedrock and detrital samples (Beltrando et al., 2015).

Ultimately, among the previous low-T thermochronometric data of the Southern Alps, the few Permian ages so far recorded are from two groups of samples consisting mostly of volcanic and detrital rocks and including one basement sample. One group of samples is located south-west of Lake Maggiore, where Permian volcanics and Jurassic sandstones give zircon (U–Th)/He ages that scatter over a very long temporal interval from the latest Carboniferous to the Late Cretaceous (Beltrando et al., 2015), indicating a low-temperature, protracted thermal history that causes variable age-resetting conditions. The second group of samples is in the Varese area and includes a 256 Ma old zircon fission-track age in a schist (Giger, 1991) and a zircon (U–Th)/He age cluster between 300 and 250 Ma combined with a Late Cretaceous age cluster in a Permian volcanoclastic rock (Beltrando et al., 2015). Thus, also this second group of samples has a complex thermochronologic record straddling age-resetting conditions.

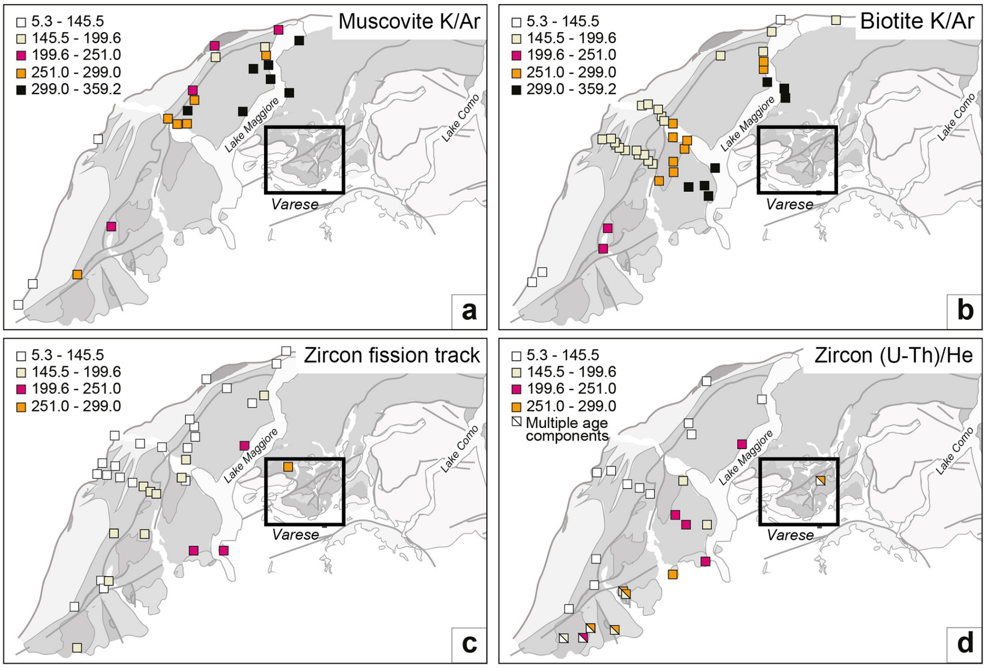


**Figure 2. (a)** Muscovite K/Ar ages compiled from McDowell (1970), Hunziker (1974), Zwingmann and Mancktelow (2004) and Wolff et al. (2012). **(b)** Biotite K/Ar ages compiled from Jäger and Faul (1960), Carraro and Ferrara (1968), McDowell and Schmid (1968), McDowell (1970), Hunziker (1974), Hurford (1986), Siegesmund et al. (2008), and Wolff et al. (2012). **(c)** Zircon fission-track ages compiled from Hurford (1986), Bertotti et al. (1999), Siegesmund et al. (2008) and Wolff et al. (2012). **(d)** Zircon (U–Th)/He ages compiled from Wolff et al. (2012) and Beltrando et al. (2015). Sample with multiple age components are from detrital rocks and partially reset basement rocks (Beltrando et al., 2015).

## 3 Methods

### 3.1 Tectono-stratigraphy and thickness analysis

In this work, we focused on the tectonostratigraphic evolution from the Carboniferous to the Late Triassic, encompassing the end of the Variscan cycle and the onset of the Alpine cycle. This reconstruction builds on prior studies of the tectono-stratigraphy of the Southern Alps (e.g. Bernoulli, 1964; Bertotti et al., 1993; Gaetani et al., 1998; Berra et al., 2009; Cassinis et al., 2012) and on the results from our geological mapping that we used to measure stratigraphic successions to identify crosscut relationships among structures and to map key horizons and unconformities. Geologic structures were extrapolated at depth by means of a series of geological cross-sections (see Sect. 4.1 for the tectono-stratigraphy).

A quantitative approach based on a thickness analysis was adopted for the reconstruction of the basin morphology during the inception of the rifting Alpine stage. Specifically, we focussed on the Middle Triassic and on the development of a fault-bounded basin within the Varese area at that time, as we identified this geologic event as essential to understand the onset of the Alpine cycle. We built 25 geological cross-sections (locations in Fig. 4c) that informed a 3D geologic model, developed using the MOVE software (courtesy of Petroleum Experts Ltd). The model is composed of mesh surfaces representing the top horizons of stratigraphic units and fault surfaces. These mesh surfaces are available as a 3D pdf file in the Supplement (S1). The horizons from the geological cross-sections were interpolated within each fault-bounded structural block and across sections, by means of a spline interpolation method, to minimise curvature away from fault zones. Each structural block was then progressively restored using a 3D flexural slip unfolding algorithm. As a key horizon for the Alpine tectonic restoration, we used the oldest post-rifting available horizon (i.e. the Aptian Unconformity, the top of the Maiolica Fm.) that we assumed to be horizontal all across the study area. Finally, the syn-rift fault displacements were restored using a 3D simple shear un-faulting method (Withjack et al., 1995). The restored geometries were then compared to structural data from fault surfaces (results in Sect. 2.2). Finally, from the 3D geologic model, we derived an isopach 2D contour map, projected on the restored top of Middle Triassic surface.

### 3.2 Kinematic analysis

Kinematic data were collected along the early Permian–Middle Triassic fault systems to determine the orientation of the best-fit moment tensor solution, enabling us to calculate the paleo-strain orientation for each tectonic phase.

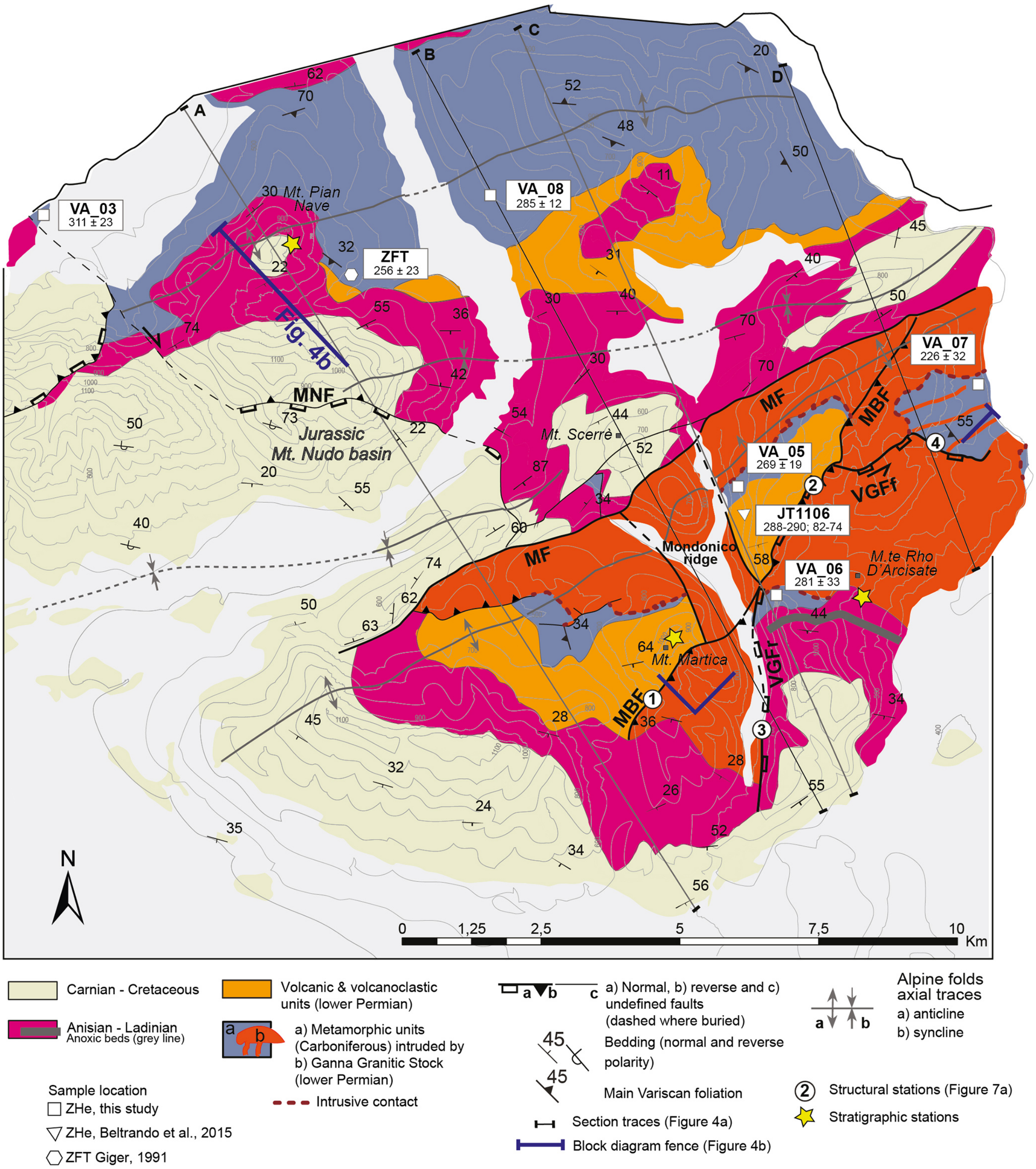


**Figure 3.** Geological map of the study area (modified after Scaramuzzo et al., 2022). ZHe: zircon (U–Th)/He; ZFT: zircon fission-track. Fault codes: MF, Marzio Fault; MBF, Martica–Boarezzo Fault; VGFr, Valganna Fault ramp segment; VGFf, Valganna Fault flat segment. The Mt. Nudo basin is Jurassic in age (Kalin and Trümpy, 1960).

We calculated moment tensor summations of the strain axes (i.e. E1E2E3; extension positive), as implemented in FaultKin 8 (https://www.rickallmendinger.net/faultkin, Allmendinger, 2024). For a complete discussion of the assumptions and limitations of these methods, see Marrett and Allmendinger (1990). We inverted the fault slip data from their present-day orientation, and, in order to account for the later Alpine tectonics, we restored the obtained fault plane solution according to the bedding plane (S0), extrapolated from the nearest sector, along strike.

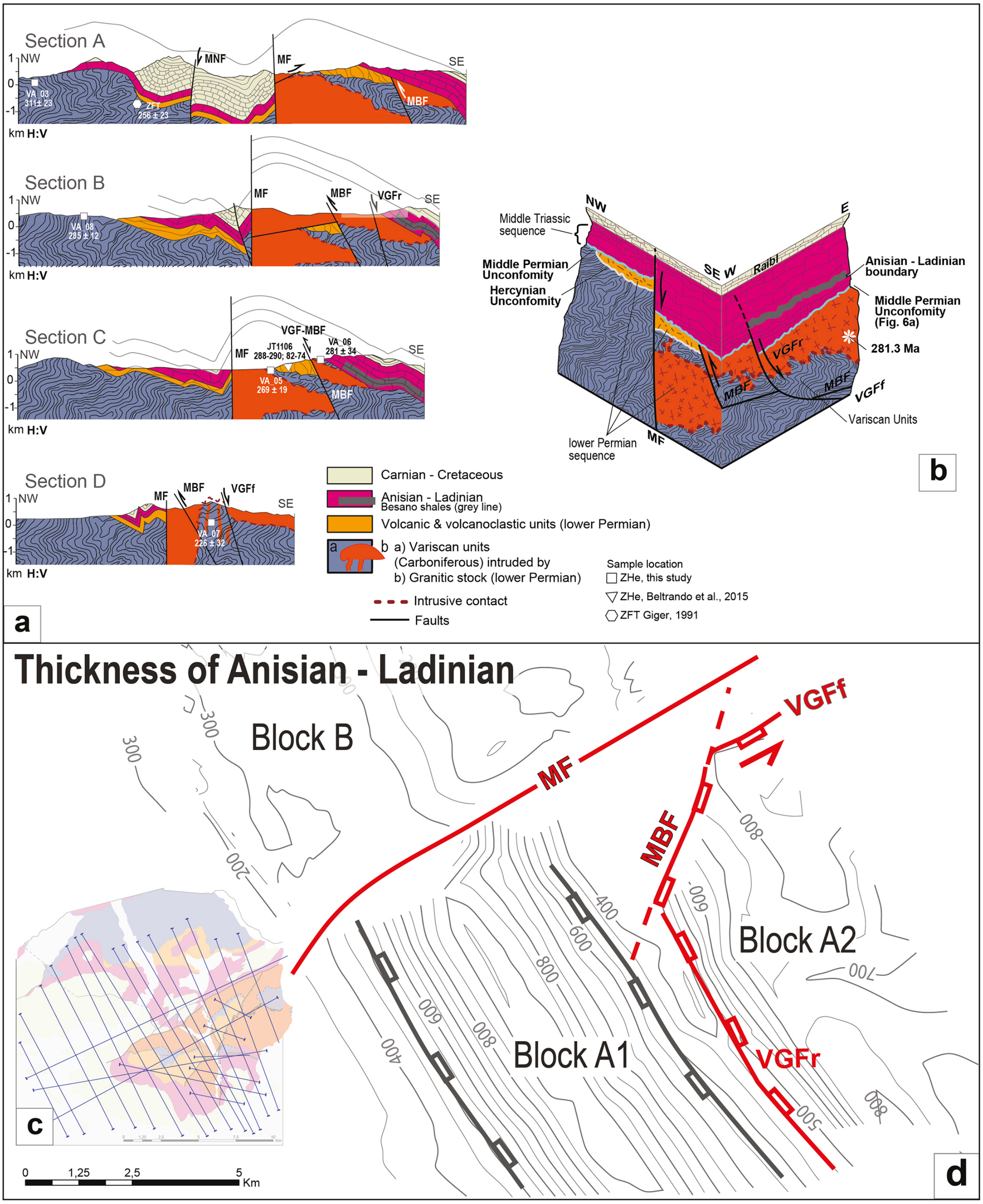


**Figure 4.** **(a)** Geological cross-sections across the study area and traces of the cross-sections in Fig. 3. Codes: MBF, Martica–Boarezzo Fault; MNF; Monte Nudo Fault; MF, Marzio Fault; VGF, Valganna Fault; ZHe, zircon (U–Th)/He; ZFT, zircon fission-track. **(b)** Tectono-stratigraphic block diagram of area (restored at Carnian). **(c)** Traces of the geological cross-sections' grid used to build the 3D geological model of the area. **(d)** Isopach map of the Middle Triassic sequence (Anisian–Ladinian), after restoration; outcropping faults are represented with red lines.

### 3.3 Thermochronology

#### 3.3.1 Zircon (U–Th)/He dating

We collected samples from gneiss and micaschists of the Variscan basement in the hanging walls and footwalls of major faults. Zircon (U–Th)/He (ZHe) analysis was conducted at ETH Zurich. Zircon grains were first extracted from crushed samples using conventional methods of heavy liquid and magnetic separation. Euhedral zircons with widths of >60 µm were then selected from each sample under a polarised stereo-microscope. Each grain was photographed to measure its dimensions for the calculation of alpha-ejection correction factor (FTK) following Ketcham et al. (2011). Afterwards, each zircon was packed in Niobium foil and loaded into an ultra-high vacuum sample chamber. $^{4}He$ amounts were determined by outgassing with a diode laser at 1090 °C for 45 min and measuring the released gas on a magnetic sector-field mass spectrometer equipped with a Baur-Singer ion source in static vacuum. A second extraction was conducted for each grain at 1110 °C for 22 min. A third extraction was performed at 1130 °C for 22 min for the grains, which still had high fractions of $^{4}He$ released from the second extraction (>1 %). Outgassed zircons were then transferred into Teflon vials, spiked with $^{233}U$ and $^{230}Th$ mixed solution, and dissolved first at 225 °C for 72 h in a concentrated mixture of HF and $HNO_3$ and then in concentrated HCl at 200 °C for 24 h to ensure dissolution of refractory fluoride salts. U and Th concentrations of each final solution were measured on an inductively coupled plasma mass spectrometer (ElementXR). To verify the accuracy of date estimates and monitor intrasample dispersion, six zircons from the Fish Canyon Tuff were processed alongside the samples. These zircons were not used for calibration purposes. They yielded a mean FTK age of 27.2 ± 1.5 Ma (± standard deviation (1 s); Supplement Table S2), which are consistent with the recommended eruption age of 28.0–28.2 Ma (Boehnke and Harrison, 2014).

#### 3.3.2 Thermochronologic modelling

To evaluate the thermal effect related to the granitic intrusion occurring in the area, we calculated the heat transfer from the cooling granitic stock to the surrounding crust by means of a simple 1D transient diffusion equation. We assumed that the magmatic body emplacement occurred instantaneously and that the size of the stock was relatively small with respect to the thickness of the intruded crust (Ehlers et al., 2003). With these conditions the temperature ($T$) of any point at a given distance from the intrusion ($z$) with time ($t$) is provided by Carslaw and Jaeger (1959):

$$T\left(z,t\right)=T_b+\frac{T_{\mathrm{i}}-T_b}{2}\left[\operatorname{erf}\left(\frac{L/2-z}{2\sqrt{\alpha t}}\right)+\operatorname{erf}\left(\frac{L/2+z}{2\sqrt{at}}\right)\right],$$

where $T_{\mathrm{i}}$ is the temperature of the intrusion and $T_b$ the one of the crust, $L$ is the intrusive body thickness, and $a$ is the thermal conductivity coefficient. Erf is the error function (Abramowitz and Stegun, 1970).

## 4 Results

### 4.1 Tectono-stratigraphy

The succession outcropping in the study area is comprised between the Carboniferous and the Cretaceous (Fig. 3). We focused on the lower Permian–Middle Triassic succession as it records the transition between the Variscan and the Alpine cycles. Tectono-stratigraphic results are summarised in the following sections and illustrated in the geological map in Fig. 3 and in the sections and tectono-stratigraphic scheme of Fig. 4.

#### 4.1.1 The lower Permian succession

The lower Permian succession is composed of (i) the Ganna Granitic Stock, intruded at shallow levels within the Variscan basement, with its intrusive contacts exposed both at the top and at the base of the stock (Figs. 3 and 4), and (ii) the volcanic and volcano-clastic units, lying on top of the basement, above the Hercynian Unconformity.

The lower Permian succession records the activity of the Marzio Fault. This is a near-vertical structure that divides the study area into northern and southern blocks along a NE–SW direction (Fig. 3). Stratigraphic sections measured on both sides of this fault (Fig. 4b) show an abrupt increase in the thickness of the lower Permian volcanic/volcanoclastic rocks from approximately 200 m in the northern fault block to about 1500 m in the southern fault block (section A in Fig. 4a, b). This fault bounds sharply to the north also the lower Permian intrusive stock and puts it in contact with pre- to lower Permian, metamorphic and volcanic rocks (Figs. 3; 4a, b). Thin dikes and sills are commonly associated with the stock, cutting through the basement south of the Marzio Fault, whereas they are absent to the north of the Fault (Bernoulli et al., 2018). To the south of the Marzio Fault, the lower Permian intrusive and extrusive rocks are also displaced by a reverse fault that we here describe for the first time: namely, the Martica–Boarezzo Fault. This is a SW-NE striking, high-angle, SE-dipping fault. This structure displaces the Ganna Granitic Stock onto the lower Permian extrusive units (sections A and C, in Fig. 4a) and abuts onto the Marzio Fault to the north-east (Fig. 3).

The middle Permian Unconformity truncates the Martica–Boarezzo Fault (Figs. 3 and 4b). Thus, the age of the Martica–Boarezzo Fault is constrained between the late early Permian and the middle Permian.

South of the Marzio Fault and north of the Martica–Boarezzo Fault, two high-angle NNW–SSE-trending faults bound a narrow structural high known as the Mondonico ridge (Fig. 3). Due to erosion, no crosscut relationship with the stratigraphic succession exists to constrain the timing of the activity of the Mondonico ridge. While the faults bounding this ridge appear to be displaced by the Martica–Boarezzo Fault, evidence for this interpretation is limited due to the extensive coverage of Quaternary deposits. Alternatively, the development of the Mondonico ridge could have occurred contemporaneously with the activity of the Martica–Boarezzo Fault. Further research is required to investigate this hypothesis in greater depth.

#### 4.1.2 The Lower–Middle Triassic succession

On top of the middle Permian Unconformity, thin, siliciclastic, Lower Triassic layers show no significant cross-cut relationship with the tectonic structures in the study area and are overlain by a thick carbonate succession that is Anisian–Ladinian in age. This succession consists of platform and intra-platform facies with a highly variable distribution. In particular, the intraplatform facies (i.e. the anoxic beds within the Besano and Meride Formations) pinch out to the west. At the top, this succession is closed by an almost continuous interval with constant thickness, composed by thin bedded evaporitic dolostones of Carnian age (Pizzella Fm. in Fig. 1).

The Middle Triassic succession is gently folded or involved in Alpine thrusts north of the Marzio Fault, while, to the south, it is displaced by the Valganna Fault (Fig. 3) with an apparent left-lateral separation. The Valganna Fault is limited to the hanging wall block of the Martica–Boarezzo Fault, never displacing the latter and partly re-activating a small segment of the inherited reverse fault. The upper tip of the Valganna fault is sealed by the Carnian (Fig. 3).

This structure is a normal fault presently describing an arcuate trace in map view due to Alpine tilting and erosion. Presently, the Valganna Fault is split into two segments with different orientation: a southern one, sub-vertical and striking N–S (VGFr in Fig. 3 and sections B and C in Fig. 4a), and a northern one, dipping ca. 60° with an ENE–WSW strike (VGFf in Fig. 3, and section D in Fig. 4a). If tilted back to their original attitude (S0 N170/40, measured ca. 1 km south of the VGFf), the two segments represent the shallow ramp (VGFr) and a slightly deeper, less steep sector (VGFf) of the Valganna Fault, respectively. The apparent left-lateral separation results from a combination of Alpine deformation and original Middle Triassic normal displacement. Specifically, after restoring and unfolding the Alpine deformation, a substantial residual normal offset remains along the Valganna Fault. The magnitude of this offset aligns with the thickness change that we measured across the fault. In fact, across VGFr, the Anisian–Ladinian succession shows a thickness increase from 500 m to the east, up to 800 m, to the west (sections B and C in Fig. 4a and c). VGFf presently dips at a high angle to the SSE (sections C and D in Fig. 4a) but its restored dip is close to 30°. It displaces the Ganna Granitic Stock, in the hanging wall, against the basement, in the footwall (Fig. 3, section D in Fig. 4a). At the junction between VGFf and VGFr, the Valganna Fault negatively inverts the inherited Martica–Boarezzo Fault. To the south, the Valganna Fault is clearly truncated by the top of the Anisian–Ladinian succession (Fig. 3).

The Middle Triassic isopach map (Fig. 4d) shows a variable basin topography in the study area. Differential subsidence, up to 600 m, occurs across the Marzio Fault between the northern block (block B in) and the more subsiding southern block (Block A in Fig. 4d). The southern block features two narrow NW–SE elongated basins indicated as A1 and A2 in Fig. 4d. The thickness analysis indicates that A1 and A2 are separated by a horst, are bounded by faults on the west and on the east, and accommodated up to 800 m thick Anisian–Ladinian sediments. The thickness analysis also suggests that the Valganna Fault bounds the eastern basin (A2) on the west and on the north, and the Marzio Fault bounds the western basin (A1) to the north.

### 4.2 Fault kinematics and field evidence

In the field, the faults described in Sect. 4.1 display the same crosscut relationship derived from mapping in several locations, including still-preserved kinematic indicators.

We measured kinematic data (i) along the Martica–Boarezzo Fault where it cuts through the Ganna Granitic Stocks and the overlying Permian calc-alkaline succession (structural stations 1 and 2 in Fig. 3), (ii) along the Valganna Fault across the Ladinian carbonate platform rocks, and (iii) along the contact between the basement and the Ganna Granitic Stock (structural stations 3 and 4 in Fig. 3).

Along the Martica–Boarezzo Fault, fault steps and slickenlines indicate a reverse dip-slip sense of motion (Fig. 5a, b) and sets of $P$- and $R$-Riedel shears with related slickenlines that indicate right-lateral transpressive movements (Fig. 5c, d). These kinematic indicators are associated with syn-kinematic quartz veins and porphyric dikes (Fig. 5c, e). At places, reverse faults show evidence of a negative inversion, with overprinting steps and slickenlines, or a clear crosscut relationship with younger normal faults, displacing the reverse ones (Fig. 5c).

The inversion of fault-slip data (Fig. 7b, c) indicates a strike slip to transpressive fault plane solution for the Martica–Boarezzo Fault, with a maximum shortening axis (i.e. strain axis E3) oriented ca. NW–SE (Fig. 7b, c).

The Valganna Fault core is exposed locally, where it displaces the Anisian–Ladinian succession showing fault breccia to fault gauge up to ca. 10 m thick (Fig. 6f), surrounded by a discrete damage zone tens of metres wide . Fault slip data along the Valganna Fault (Fig. 7a) point to an extensional to slightly transtensional kinematics. High-angle, SE-dipping fault surfaces are most common along the ramp segment of the Valganna Fault, which features three sets of normal faults and strike-slip faults (Fig. 7b). The slip inversion

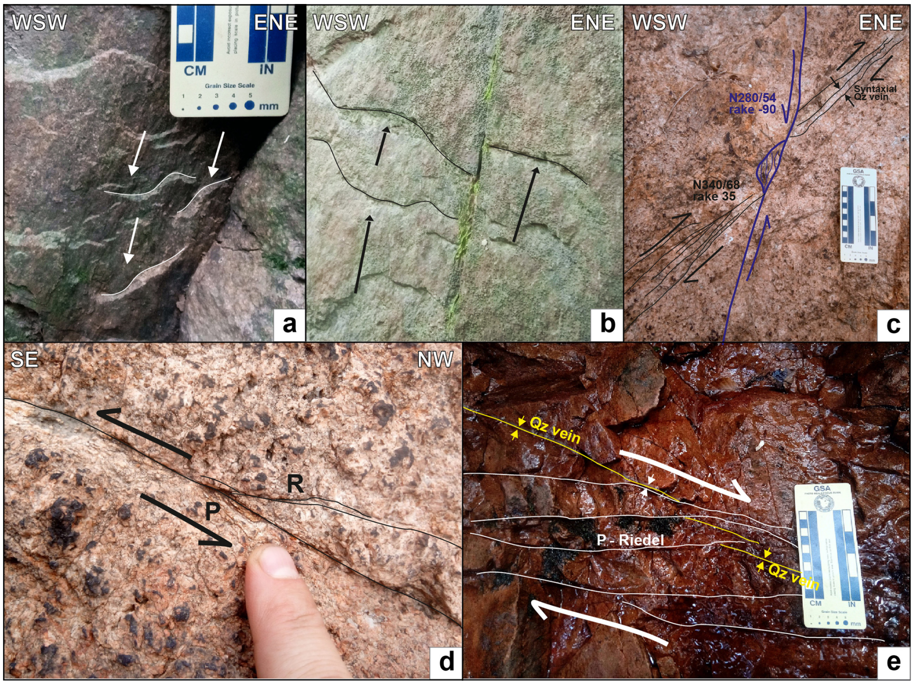


**Figure 5.** Representative kinematic features of the Martica–Boarezzo Fault; all the pictures are taken from the Ganna Granitic Stock. **(a, b)** Hanging wall and footwall, respectively, with high-angle reverse faults marked by fault steps and slickenlines. **(c)** High-angle transpressive fault, associated with quartz veins and a thin quartz-porphyric dike, cut by a later high-angle normal fault (in blue). **(d)** Left-lateral strike slip fault in the hanging wall of the MBT: note the associated *R* and *P* fractures. **(e)** Right-lateral strike slip fault: note the associated *P* fractures and offset quartz veins.

of these faults, after backfolding, indicates E–W extension (Fig. 7c). Along the flat segment of the Valganna Fault, two main sets of normal and transtensive faults (Fig. 7a) indicate WNW–ESE-directed extension, after backfolding (Fig. 7b).

## 4.3 Thermochronology

### 4.3.1 (U–Th)/He dates

Five samples, out of nine, from gneiss and micaschists provided good quality zircons for (U–Th)/He (ZHe) dating. Sample mean ages and their 1 standard deviation (1 s) are given in Table 1 and reported both in the geological map (Fig. 3) and in the geological cross-sections (Fig. 4). Sample details are outlined in the Supplement Table S2, presenting measured quantities of U, Th, Sm and He along with their uncertainties calculated from 1 standard deviation (1 s) of the measurements. Additionally, the table includes single grain ages and their corresponding propagated measurement uncertainties (1 s). Three samples (VA05, VA06, VA07) are in the hanging wall of the Marzio Fault close to the Ganna Granitic Stock, and two samples (VA03 and VA08) are from the block that acted as footwall of the Mt. Nudo Fault and of the Marzio Fault (Fig. 2). One sample (VA07) includes 11 grains with a mean Late Triassic ZHe age of 226 ± 32 Ma (1 s, 14%); three samples (VA05, 06, and 08) include four to seven grains with mean ZHe ages in the range from 268 to 284 Ma, which is early Permian, and with standard deviations (1 s) varying from 19 Ma to 34 Ma (from 4 % to 12%); finally, one sample (VA03) with four grains gives a late Carboniferous age of 311 ± 23 Ma (1 s, 7 %).

The standard deviation of samples VA06 and VA07, 12 % and 14 %, respectively, is significantly higher than the 6 % of the Fisch Canyon Tuff zircons, which were processed together with our samples. This observation suggests that samples VA06 and VA07 could be over-dispersed. Age dispersion can reflect either different zircon features like, for instance, differences in grain size, in radiation damage, and in U and Th distributions, or simply analytical uncertainties that cannot be accounted for. Zircon dimensions control the size of the He diffusion domain, and this results in positive correlations among ZHe closure temperature, zircon dimensions and ZHe ages (e.g. Reiners and Brandon, 2006). The radiation damage accumulated in zircons also controls the closure temperature and, in turn, is controlled by the zircon U and Th concentrations and thermal history (Shuster et al., 2006). The effect of the radiation damage on the ZHe closure temperature is non-linear, and it can be identified by plotting ZHe ages against the effective U concentration (eU), which is a proxy for the radiation damage (Gautheron et al., 2009). Additionally, non-homogeneous U and Th distribution in zircon can result in an inaccurate alpha-ejection correction and in


**Figure 6. (a)** Middle Permian Unconformity highlighted by the contact between the lower Permian Ganna Granitic Stock and the Anisian Bellano Fm. **(b)** Detail of the base of the Bellano Fm. **(c–f)** Mesoscopic structural features of Valganna Fault.

**Table 1.** Summary of (U–Th)/He age results; see Fig. 1 for sample location on map and Fig. 7 for locations in geological cross-sections.

| Sample code | Coordinates (lat, long) – WGS84 | Elevation (m a.s.l.) | N. grains | Age (Ma) | Error; 1 s (Ma) |
|---|---|---|---|---|---|
| VA03 | 45.956203; 8.667739° | 205 | 4 | 310.53 | 23.33 |
| VA05 | 45.911899; 8.830069° | 563 | 7 | 268.82 | 19.32 |
| VA06 | 45.892824; 8.840748° | 796 | 5 | 280.92 | 33.73 |
| VA07 | 45.929817; 8.886418° | 358 | 11 | 225.74 | 32.38 |
| VA08 | 45.956942; 8.770584° | 340 | 4 | 284.76 | 12.53 |

age dispersion (Hourigan et al., 2005). All these effects can occur at the same time making it difficult to separate them. In our samples, we did not correct for non-homogeneous U and Th distributions, as this would require additional, non-routine measurements, However, we observe a slightly negative age–eU relationship in VA07 and no correlation with grain size in any sample (Fig. 8). Thus, the age overdispersion in VA06 and VA07 could relate partly to the effect of radiation damage and partly to other effects that we cannot account for.

We used the Welch $t$ test (Welch, 1947) to test whether our samples have equal ZHe mean ages: results (Table 2) indicate that the Triassic sample is younger than the other samples; the three early Permian samples have equal ZHe ages, and the late Carboniferous sample has a mean equal to two out of three of the early Permian samples and could be slightly older than the third sample.

#### 4.3.2 The effect of the granitic intrusion on the thermochronologic record

The proximity of some of our samples to a granitic intrusion, i.e. the Ganna Granitic stock, which is early Permian in age (281.3 ± 0.5 Ma; Schaltegger and Brack, 2007), suggests

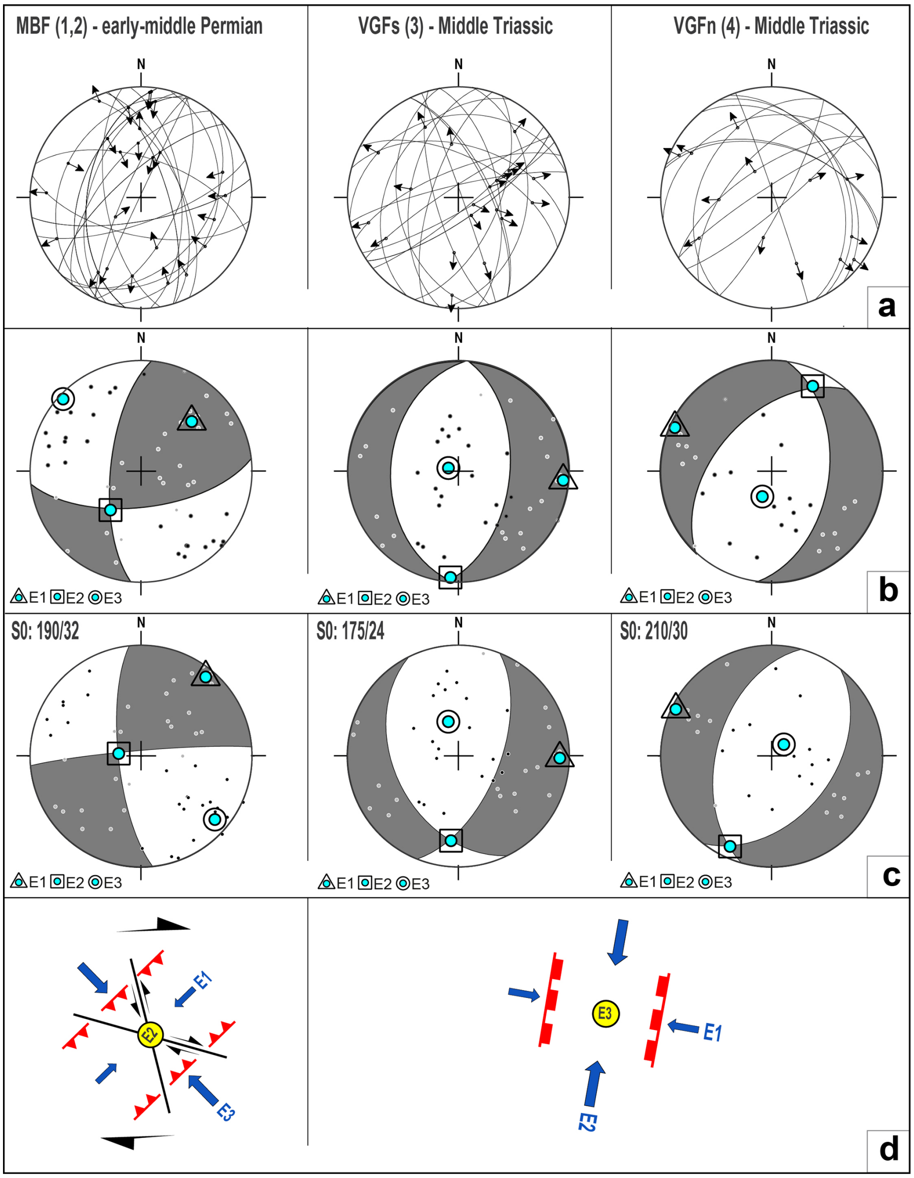


**Figure 7.** Fault slip data and inversion: **(a)** fault slip data along the faults described in the text (see Fig. 3 for the location of the structural stations). **(b)** Kinematic inversion, where $P$ and $T$ axes and the best fit fault plane solutions are represented. **(c)** Kinematic inversion after restoration to the nearest bedding orientation (S0). Codes: MBF: Martica–Boarezzo Fault; VGFr: Valganna Fault – ramp segment; VGFf – Valganna Fault – flat segment. **(d)** Schematic diagrams summarising the relationships between the orientations of strain axes and the strike and the kinematics of expected fault.

that post-magmatic cooling rather than cooling related to exhumation could affect the ZHe ages. Three samples (VA05, VA06 and VA07) are very proximal ($\leq 2$ km away, Fig. 3) to the Ganna granitic stock, whereas two samples (VA08 and VA03) are several kilometres from the intrusion, about 5 km and $>10$ km, respectively. Among the samples proximal to the intrusion, only two (VA05 and VA06) have ZHe ages similar to the intrusion age, whereas one sample (VA07) has a Triassic ZHe age. The samples far from the intrusion (VA08 and VA03) have ZHe ages similar within uncertainty to the Ganna intrusion age.

To test for the thermal effect related to the intrusion, we used a 1-D heat-transfer model at shallow depth combined with an estimate of the time–temperature conditions, at which a heating event could cause He loss in zircons. For the heat-transfer model, we assumed a background temperature ranging between 55 and 82.5 °C, consistent with a near-surface intrusion depth (i.e. less than 2 kbar; Bakos et al., 1990), an initial intrusion temperature of 650 °C and a ther-

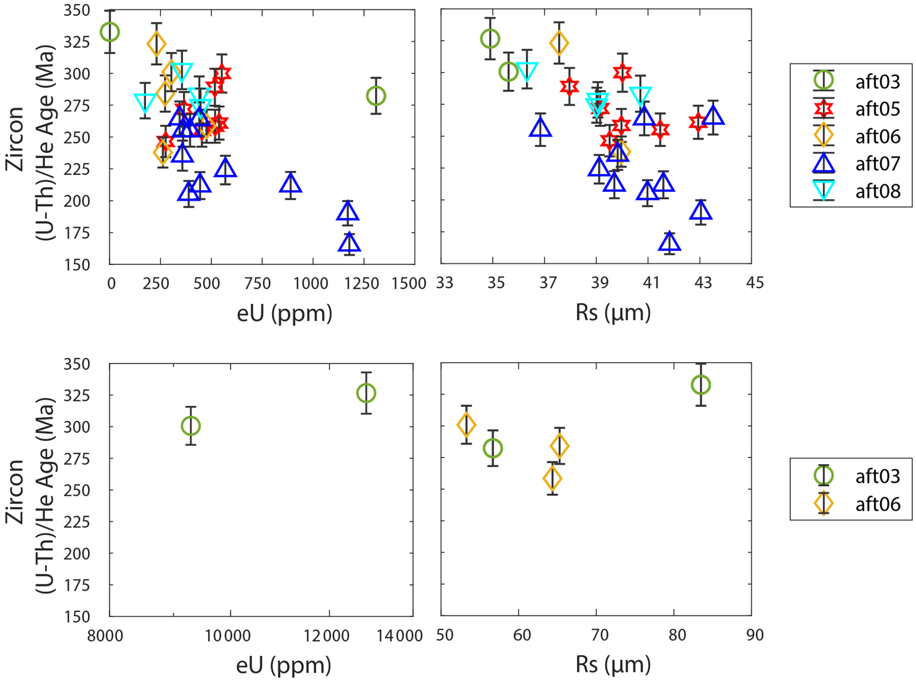


**Figure 8.** Diagram showing all zircons (U–Th)/He data plotted against effective uranium (Ue) concentrations and equivalent spherical radius (Rs). Uncertainties are 1 standard deviation.

**Table 2.** The *t* test on the obtained (U–Th)/He ages to check the probability that two samples derive from two overlapping distributions sharing the same mean. Triassic ages are highlighted in yellow, Permian in blue and Late Variscan in red, for ease of comparison.

| | | Triassic | Permian | | | Carboniferous |
|---|---|---|---|---|---|---|
| | | VA07 | VA05 | VA06 | VA08 | VA03 |
| Triassic | VA07 | – | <0.05 | <0.05 | <0.05 | <0.05 |
| Permian | VA05 | | – | 0.498 | 0.133 | <0.05 |
| | VA06 | | | – | 0.823 | 0.165 |
| | VA08 | | | | – | 0.114 |
| Carboniferous | VA03 | | | | | – |

mal diffusivity of 32 $km^2\ Myr^{-1}$ (Fig. 9). These inputs result in temperatures close to the intrusion temperature for 1 year at a horizontal distance of 1 km from the granite and temperatures in the range of 200 and to 250 °C for 0.1 Ma at 2 km distance. To calculate how long a zircon should be held at a certain temperature to cause 90 % He loss, which would cause age resetting, we used the partial loss-only He diffusion equations (Reiners and Brandon, 2006). In these equations we input average ZHe kinetic parameters (Reiners et al., 2004) and grain dimensions equal to the mean equivalent spherical radius (Rs; Supplement Table S2) of the zircons dated in this study (Rs: 45 µm). We obtained that a steady temperature close to 400 °C for 1 year results in 90 % He loss, whereas a steady temperature close to 200 °C requires at least 1 Ma time to produce 90 % He loss. Thus, the early Permian ZHe ages of VA05 and VA06, which are proximal to the intrusion, likely reflect post-magmatic cooling. In contrast, the early Permian ZHe ages of VA08 and VA03, located over 5 km from the intrusion, allow for two possible interpretations: they may record cooling related to exhumation or reflect post-magmatic cooling related to a buried, unexposed granite in the footwall of the Marzio Fault. Lastly, the cooling ages of VA07 span a range from 250 to 170 Ma – encompassing the timing of the Ganna granitic intrusion but extending into the Middle Jurassic – too wide a span to solely reflect post-magmatic cooling.

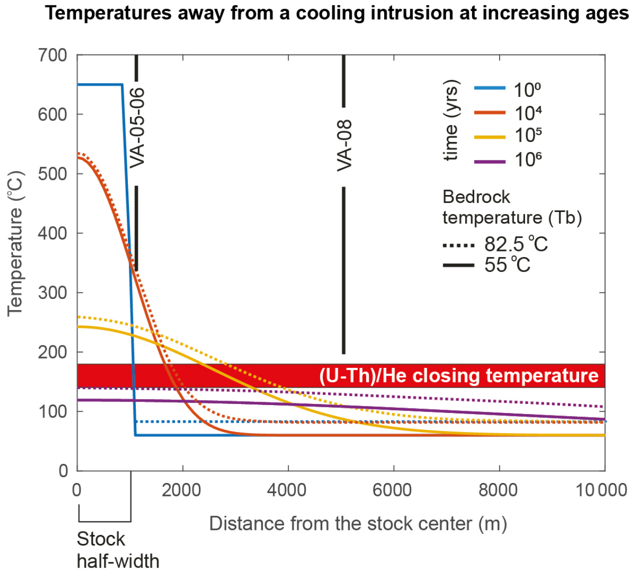


**Figure 9.** One-dimensional transient thermal response to an intrusion (half width = 1000 m). Intrusion depth was assumed to be shallow and into country rock at background temperature ranging between 55 and 82.5 °C, initial intrusion temperature of 650 °C, and thermal diffusivity of 32 $km^2$ $Myr^{-1}$.

## 5 Discussion

### 5.1 Permian thermal record

In the study area, previous thermochronologic data include a schist sample with a zircon fission-track age of 256 Ma (Giger, 1991) and a Permian volcanoclastic sample with two distinct ZHe age clusters: an older cluster between 288 and 280 Ma and a younger one between 82 and 74 Ma (Beltrando et al., 2015). The age clusters of this volcanoclastic sample indicate Permian cooling, no rift-related He-loss, and possibly some early Alpine heating. Although this sample is close to one of ours, we find no evidence of an Alpine thermal overprint in any of our samples, which collectively include 31 zircons. This suggests that the Alpine thermal overprint may be restricted locally. The complex ZHe age distribution of the volcanoclastic sample might also partially reflect its clastic nature, implying that the sample may include zircons with a long and varied geologic history that respond diversely to low-T thermal events. In contrast, the simpler, narrowly dispersed ZHe age distributions in our samples may relate to their origin in Carboniferous metamorphic rocks, which were likely metamorphosed at temperatures sufficient to anneal the inherited histories of the zircons. Alternatively, the relatively limited age distribution in our samples might reflect the small number of grains analysed per sample, potentially undersampling the full ZHe age distribution. Overall, our samples exhibit little to no post-Permian rejuvenation: three out of the five samples have mean ZHe ages that are Permian, while the remaining two samples are dated to the late Carboniferous and Late Triassic, respectively.

The Permian thermal record of several of our samples appears to be associated with the emplacement of the Ganna Granitic Stock. Two Permian ZHe ages (VA05: 269 ± 19 Ma; VA06: 281 ± 33 Ma) from basement rocks south of the Marzio Fault were thermally reset by this intrusion. These ages likely represent post-magmatic cooling, indicating that the Ganna Granitic Stock intruded Carboniferous metamorphic rocks at 281 Ma. A third sample (VA07: 226 ± 32) from nearby basement rocks has a younger, more dispersed ZHe age range (260–170 Ma) with a negative relationship with eU (Fig. 8), hinting at an additional thermal event beyond the granitic intrusion. Thus, by the early–middle Permian, rocks south of the Marzio Fault were likely at shallow crustal levels, at depths near or shallower than the ZHe closure temperature (i.e. ∼ 180 °C; Reiners and Brandon, 2006).

North of the Marzio fault, two samples show Permian (VA08: 285 ± 12 Ma) and late Carboniferous (VA03: 311 ± 23 Ma) ZHe ages. Despite being statistically similar ($T$-test, Table 2), VA08 aligns with the timing of the Ganna Granitic Stock intrusion. A 1D thermal model indicates that the thermal effect of a shallowly emplaced granitic intrusion drops rapidly both in space and time, and no field evidence suggests a granitic intrusion near VA08. While buried, unexposed granitic intrusions near VA08 are possible, given the landscape's topography, with incised valleys, the likelihood of unexposed granites is minimal. Field data indicate that during the early–middle Permian, the Marzio fault acted as a normal fault with volcanic and magmatic activity in the hanging wall. Despite no thermochronologic age offset across the fault, our data are consistent with the normal activity of the Marzio fault during the early–middle Permian. The lack of offset likely reflects the thermal overprint from the granitic intrusion, which masked the typical cooling age pattern across a normal fault, where younger cooling ages would be normally observed in the footwall (e.g. Willett et al., 2021). In this context, VA08 and VA03 record exhumation of the footwall prior to and during the emplacement of the Ganna Granitic stock, while VA05, VA06 and VA07 were thermally reset by the intrusion. The slightly older Carboniferous age of VA03 may reflect its greater distance from the Marzio Fault, consistent with the trend of younger ages in footwall rocks closer to a fault. The younger cooling age of VA07 may relate to its lower elevation in the tectonic-stratigraphic succession of the study area, near the eastern margin. This margin is near the area affected by Late Triassic–Jurassic crustal thinning, generated by a widespread thermal anomaly that affected the thermochronologic record of the basement rocks of the central Southern Alps and resulting also in the emplacement of ore deposits (Bertotti et al., 1999; Giorno et al., 2022). The ZHe age distribution of VA07, along with its negative relationship with eU (Fig. 8), suggests that this sample accumulated high radiation damage over a long residence at shallow crustal depths, with partial thermal rejuvenation possibly starting in the Triassic and persisting into the early Jurassic. Consequently, the Late Triassic–Jurassic thermal anomaly in the Southern Alps is evident only in sample VA07.

In conclusion, our thermochronologic data indicate that since the early Permian, basement rocks in the study area have been relatively stable, residing at shallow depths with minimal exposure to later thermal events. This long-term stability highlights a unique thermal history for the region, with most rocks undisturbed by major post-Permian thermal episodes, reinforcing a consistent, shallow-crustal preservation since the Permian.

### 5.2 The Variscan–Alpine cycle transition

The data presented here provide new temporal and kinematic constraints for the transition between the Variscan and Alpine cycles, particularly on the age of the earliest crustal rifting stage at the inception of the Alpine cycle and its temporal and kinematic relations to earlier tectonic phases. The tectonic and thermochronological datasets demonstrate that, in the study area, the Variscan metamorphic basement was exhumed during the early Permian, flattened by a regional-scale erosive phase, and then dissected into a continental endorheic basin, bounded to the north by the Marzio Fault. As this structurally controlled basin was progressively filled with calc-alkaline volcanic-volcanoclastic products, the upper crust was intruded at shallow depths by a sub-volcanic body, i.e. the Ganna Granitic Stock. The geometry of the volcanic deposits during this phase appears to be influenced by the tectonic control exerted by the Marzio Fault, as suggested by the apparent differential subsidence of the southern block, which is associated with the accumulation of a thicker volcanic succession. However, other factors, such as lateral variations in volcanic bed thickness, localised lava domes and paleotopography during volcanic emplacement, may also explain these variations (Colombo et al., 2025).

Further evidence highlights the Marzio Fault's structural control over the volcanic and magmatic activity during the Middle Permian. Thermochronologic data suggest exhumation of the Marzio Fault's footwall before and during the volcanic activity, aligning with its normal fault regime. Field observations from this and previous studies (Govi, 1960; Bakos et al., 1990; Bernoulli et al., 2018) support this interpretation showing that the Ganna Granitic Stock and associated dikes, which may intrude the overlying basement unit, are absent north of the Marzio Fault, suggesting magmatic activity was confined to its southern side. Although no early Permian magmatic activity is present north of the Marzio Fault, mantle-derived basic intrusions in the adjoining Ivrea-Verbano Zone to the west cut across the lower crust, linking early Permian magmatic activity in the Southern Alps to crustal thinning, astenospheric upwelling and magmatic underplating (e.g. Schaltegger and Brack, 2007). Unlike the shallow crustal rocks of the Varese area, the Ivrea Verbano Zone's lower crustal rocks were exposed to the surface through stepwise exhumation and tilting from the Jurassic through the Middle–Late Miocene (e.g. Wolff et al., 2012) with minimal impact on the study area.

Our observations are consistent with previous studies and altogether they indicate that the early Permian extensional phase undoubtedly occurred after the end of the Variscan cycle throughout the peri-Variscan terrain including the central Mediterranean area, i.e. Tuscany, Corsica-Sardinia, Calabria and Atlas (Fig. 10; e.g. Ziegler and Stampfli, 2001, Stampfli and Kozur, 2006; Cassinis et al., 2012; Cassinis et al., 2018; Ballèvre et al., 2020; Elter et al., 2020; Molli et al., 2020). Some authors interpret this massive calc-alkaline magmatism as being associated with the extension related to the back-arc opening of the Paleo-Tethys subduction zone (e.g. Visonà, 1982; Lorenz and Nicholls, 1984; Stille and Buletti, 1987; Di Battistini et al., 1988; Finger and Steyrer, 1990, 1991; Bonin et al., 1993; Doglioni, 1995; Ziegler and Stampfli, 2001; Stampfli and Kozur, 2006).

No reliable fault kinematic indicators are available in the study area to further characterise the stress orientation of the early Permian tectonic phase. Notably, the most reliable observations and datasets nearby, in this line, indicate that extensional detachment faults and pull-apart transtensional basins come with crustal thinning and high temperature-low pressure metamorphism widespread in all the Southern Alpine domain and the central Mediterranean area, i.e. Corsica, Sardinia and Calabria (e.g. Pohl et al., 2018; Roda et al., 2019; Zanchi et al., 2019; Molli et al., 2020; Festa et al., 2020; Locchi et al., 2022). While a discussion regarding the geodynamic nature of the early Permian extensional phase may be somewhat speculative based on our data, our observations unequivocally show a lack of continuity between the early Permian rifting and the Mesozoic Alpine Tethys rifting (Fig. 10). The early–middle Permian geologic record in our study area attests to the shifting from a rifting phase to a transcurrent phase and to the development of the middle Permian Unconformity. Indeed, the activity of the Martica–Boarezzo Fault and Mondonico ridge is consistent with the observation by Cadel (1986) and Gretter et al. (2013) of folded lower Permian deposits in the central Southern Alps suggesting a middle Permian transcurrent tectonic regime and with paleomagnetic (Muttoni et al., 2003, 2009) and stratigraphic data (Cassinis et al., 2012; Gretter et al., 2013; Cassinis et al., 2018;). To our knowledge, the Martica–Boarezzo Fault and Mondonico ridge represent a direct observation of structures related to the middle Permian transcurrent phase testifying to a regional-scale significance of this event. Some studies suggested that at this time there was indeed a change in the plate configuration from Pangea A to Pangea B between Gondwana and Laurasia (Muttoni et al., 2003, 2009, and references therein), while other studies suggested that this transcurrent phase is related to a dextral megashear system that was active during the oblique subduction of the Paleo-Tethys and the opening of the Neotethys Ocean (e.g. Cassinis et al.,

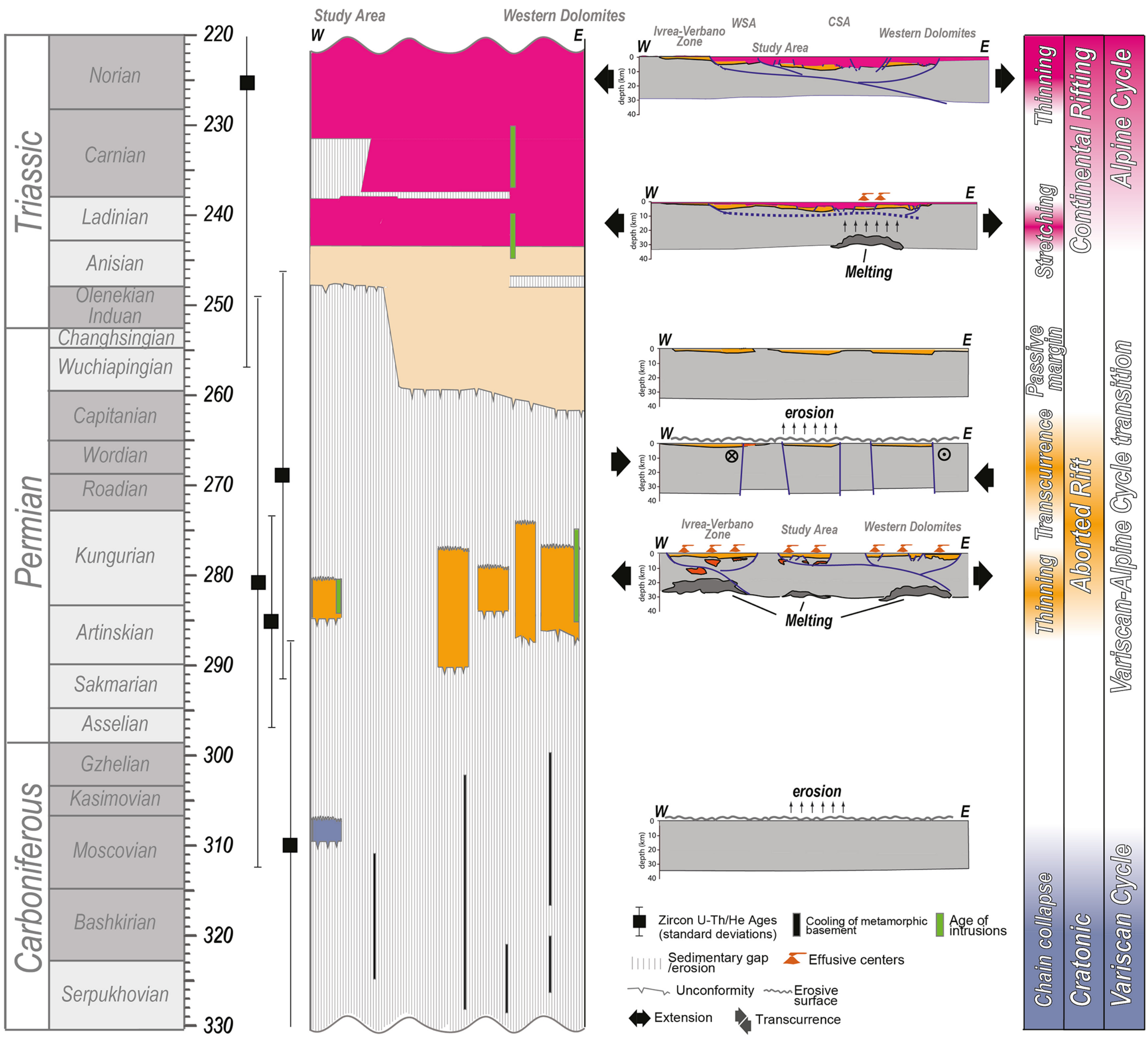


**Figure 10.** Conceptual and summary scheme of the Variscan–Alpine cycle transition as constrained in this work and from other works (WSA, Western Southern Alps; CSA, Central Southern Alps): chronostratigraphic scheme redrawn after Schaltegger and Brack (2007), Berra et al. (2009), Cassinis et al. (2012), Gretter et al. (2013), Beltrando et al. (2015), and Cassinis et al. (2018). Sections of the former Southern Alps redrawn after Beltrando et al. (2015).

2012; Gretter et al., 2013; Cassinis et al., 2018; see Torsvik and Cocks, 2004 for a complete discussion). However, the discussion supported by our dataset does not favour either of the two hypotheses.

## 5.3 The Alpine cycle inception

The end of the middle Permian transcurrent phase is marked by the onlap of the late Permian–Early Triassic siliciclastic wedge related to the marine ingression of the Paleo-Tethys from the east (Fig. 10; e.g. Bernoulli, 2007), and it is followed by a renewed phase of extension that evolved through several stages. Early Triassic units are paraconcordant with the overlying Middle Triassic ones. The only evidence for an Early Triassic tectonic activity is coming out from barite-rich veins, associated with hydrothermalism, which cut through the Lower Triassic and are sealed by the Middle Triassic, consistent with other observations in the Southern Alps (e.g. Martin et al., 2017).

During the first stage, in our study area, the Middle Triassic tectonostratigraphic data constrain a significant increase in subsidence that allowed the accommodation of up

800 m thick platform carbonate alternating with intraplatform basinal sediments. Subsidence was associated with E–W-oriented extension that was controlled by the activity of the Valganna Fault and that resulted in the dissection of the depocentre into sub-basins. The brittle nature of the ramp and flat segments of the Valganna fault suggests that extension at this time was distributed within the shallower zone of the upper crust.

The Middle Triassic extensional phase has been interpreted as related to the far field effect of the Meliata–Maliac oceans (e.g. Castellarin et al., 1988; Ziegler and Stampfli, 2001; Stampfli and Kozur, 2006; Armienti et al., 2003; Zanetti et al., 2013; Beltrando et al., 2015) or as the onset of the Alpine-Tethys opening (e.g. De Min et al., 2020; Real et al., 2023).

Finally, in the second stage, during the Late Triassic, extension was associated with localised lithospheric normal faulting that ultimately led to crustal thinning and break-up (e.g. Bertotti et al., 1993; Gaetani, 2010).

In the Late Triassic–Early Jurassic, extension continued with an E–W direction, but localised onto few master faults located outside our study area, both to the west (Mt. Nudo Basin; Fig. 1) and to the east (Lombardian Basin; e.g. Bernoulli, 1964; Bertotti et al., 1993), where kilometre-thick syn-rift sequences are preserved.

To the east of our study area, the Late Triassic–Jurassic crustal thinning produced a widespread thermal anomaly that affected the thermochronologic record of the basement rocks of the central Southern Alps and emplacement of ore deposits (Bertotti et al., 1999; Giorno et al., 2022). In our study area, the thermal overprint is evident in only one of our samples (VA07), situated in the easternmost region, at the lowest elevation, and within the deepest layers of the tectonic–stratigraphic sequence.

Thus, altogether our data support the idea that the Ladinian–Carnian extensional phase predates crustal thinning that started in the Norian (e.g. Fig. 10; Bertotti et al., 1993; Gaetani, 2010). In this view, deformation in the Ladinian–Carnian was rather distributed, resulting in a modest amount of extension concentrated within the upper crust (Fig. 10; Mohn et al., 2010, 2011, 2012; Peron-Pinvidic et al., 2013; Nalibof et al., 2017), whereas from the Norian extension it was localised along a few lithospheric detachment faults and led to crustal thinning (Fig. 10; Peron-Pinvidic et al., 2013; Nalibof et al., 2017). The co-axiality that we observed between the extensional events in the Ladinian–Carnian and the following ones supports the idea of a continuity of the geodynamic setting from the Middle Triassic through the Jurassic. This inference is concordant with the evolution of extension as proposed by previous studies in the central Southern Alps (e.g. Bertotti et al., 1993; Gaetani, 2010). This view is also supported by the geochemical data from magmatic rock in the Dolomites, indicating that the Ladinian–Carnian magmatism in the eastern Southern Alps was related to the lithosphere thinning and mantle upwelling due to rifting events that ultimately caused the break-up in the Late Triassic–Early Jurassic (De Min et al., 2020).

## 6 Conclusions

This study provides new constraints on the Variscan–Alpine cycle transition, a period relatively poorly documented within the European Southern Alps. Our data shed light on the transition from the early Permian rifting to the first inception of Triassic crustal extension, through a phase of transcurrent tectonics, previously undocumented in the study area.

In the framework of a regional perspective, the main findings of this work are as follows:

– During the early Permian, a first rifting stage resulted in the accumulation of a thick pile of volcanic and volcano-clastic successions, deposited in a structurally controlled endorheic basin. At the same time, the emplacement of a fault-bounded intrusive stock at shallow depths caused the sudden heating of the surrounding basement rocks, followed by a later cooling at shallow crustal levels where they resided for the rest of their time.

– The sudden cessation of magmatic activity, followed by transcurrent tectonics (early p.p. – middle Permian) and a later regional-scale erosion (middle Permian), marks a distinct discontinuity in the regional Permo-Triassic evolution, that is the conclusion of a first cycle of crustal rifting and the shift toward the successive Alpine cycle.

– At the Middle Triassic, the inception of a second rifting event, here documented along a well-exposed normal fault, resulted in the exhumation of the fault footwall, as recorded by thermochronological dates, the subsidence of the fault hanging wall with drowning of the carbonate platform and development of a fault-bounded anoxic basin.

– It is suggested that the Middle Triassic extension could represent the stretching phase related to the onset of the Alpine Tethys rifting.

The main implications of our findings are that the onset of the Alpine cycle dates to the Middle Triassic and that there is no continuous Permo-Triassic extension, as previously suggested by other authors (e.g. Winter and Bosellini, 1981), but there are multiple and distinct stages of rifting.

*Code and data availability.* Fault slip data inversion was calculated using FaultKin v.8 software (https://www.rickallmendinger.net/faultkin, Allmendinger, 2024). Thickness analyses were performed using the MOVE software (IPM v13.0 software suite, courtesy of Petroleum Experts Ltd). 3D mesh surfaces are available as a 3D pdf file in the Supplement (File S1). (U–Th)/He (ZHe) analysis results are available in the Supplement (Table S2) of this article. The geological map was created with QGIS 3.28.11 (https://qgis.org/it/site/, QGIS Association, 2024), and it is shown in Fig. 3 of this article.

*Supplement.* The supplement related to this article is available online at https://doi.org/10.5194/se-16-619-2025-supplement.

*Author contributions.* Conceptualisation: ES, FAL, MGF. Fieldwork and sample collection: ES, FAL. Data collection: MGF, CM. Data analysis: ES, FAL, MGF, CM. Methodology: ES, FAL, MGF, CM. Writing (original draft): ES, FAL, MGF. Writing (review and editing): ES, FAL, MGF, CM. All authors read and approved the final paper.

*Competing interests.* The contact author has declared that none of the authors has any competing interests.

*Disclaimer.* Publisher's note: Copernicus Publications remains neutral with regard to jurisdictional claims made in the text, published maps, institutional affiliations, or any other geographical representation in this paper. While Copernicus Publications makes every effort to include appropriate place names, the final responsibility lies with the authors.

*Acknowledgements.* Emanuele Scaramuzzo and Franz A. Livio would like to thank Andrea Di Capua and Michela Colombo their help with the fieldwork as well as fruitful consultations about the Permian volcanic evolution of the area. Emanuele Scaramuzzo acknowledges Paola Manzotti and Michel Ballèvre for the discussions about Variscan–Permian evolution of the Alpine and central Europe area and much more. We acknowledge Andrea Festa for commenting on an early version of this paper. We wish to thank Chris Morley and two anonymous reviewers for their constructive and helpful comments. Federico Rossetti, Virginia Toy and Florian Fusseis are thanked for the editorial handling.

*Financial support.* The geological mapping and the structural analysis were part of the PhD project of Emanuele Scaramuzzo.

*Review statement.* This paper was edited by Florian Fusseis and Virginia Toy and reviewed by Chris Morley and two anonymous referees.

## References

Abramowitz, M. and Stegun, I. (Eds.): Handbook of Mathematical Functions, Dover Publications, New York, USA, ISBN 978-0-486-61272-0, 1970.

Allmendinger, R.: FaultKin 8 [code and data set], https://www.rickallmendinger.net/faultkin, last access: 3 April 2024.

Armienti, P., Corazzato, C., Groppelli, G., Natoli, E., and Pasquare, G.: Geological and petrographical study of Montecampione Triassic subvolcanic bodies (Southern Alps, Italy). Preliminary geodynamic results, B. Soc. Geol. Ital., 2, 67–78, 2003.

Baggio, P. and De Marco, L.: La serie basale tardo-paleozoica del Varesotto e le mineralizzazioni ad uranio della Valganna, Comitato nazionale per le ricerche nucleari – Studi Ricerche Divisione Geomineraria, 3, 15–103, 1960.

Bakos, F., Del Moro, A., and Visona, D.: The Hercynian volcano-phitonic association of Ganna (Lake Lugano, Central Southern Alps, Italy), Eur. J. Mineral., 2, 373–384, https://doi.org/10.1127/ejm/2/3/0373, 1990.

Ballèvre, M., Camonin, A., Manzotti, P., and Poujol, M.; A step towards unraveling the paleogeographic attribution of pre-Mesozoic basement complexes in the Western Alps based on U–Pb geochronology of Permian magmatism, Swiss J. Geosci., 113, 12, https://doi.org/10.1186/s00015-020-00367-1, 2020.

Barth, S., Oberli, F., and Meier, M.: Th-Pb versus U-Pb isotope systematics in allanite from co-genetic rhyolite and granodiorite: Implications for geochronology, Earth Planet. Sc. Lett., 124, 149–159, 1994.

Beltrando, M., Stockli, D. F., Decarlis, A., and Manatschal, G.: A crustal-scale view at rift localization along the fossil Adriatic margin of the Alpine Tethys preserved in NW Italy, Tectonics, 34, 1927–1951, https://doi.org/10.1002/2015TC003973, 2015.

Berger, A., Mercolli, I., Kapferer, N., and Fügenschuh, B.: Single and double exhumation of fault blocks in the internal Sesia-Lanzo Zone and the Ivrea-Verbano Zone (Biella, Italy), Int. J. Earth Sci., 101, 1877–1894, https://doi.org/10.1007/s00531-012-0755-6, 2012.

Bernoulli, D.: Zur Geologie des Monte Generoso: (Lombardische Alpen); ein Beitrag zur Kenntnis der südalpinen Sedimente, Beitr. Geol. Karte Schweiz, N. F., 118, 1–134, 1964.

Bernoulli, D.: The pre-Alpine geodynamic evolution of the Southern Alps: a short summary, Bulletin für angewandte Geologie, 12, 3–10, 2007.

Bernoulli, D., Ambrosi, C., Scapozza, C., Stockar, R., and Schenker, F., Gaggero, L., Antognini, M. and Bronzini, S.: Foglio 1373 Mendrisio (parte Est) con parte Ovest del foglio Como. – Atlante geologico della Svizzera 1: 25 000, Note esplicative, in: Ufficio federale di topografia, edited by: Dall'Agnolo, S., CH-3084 Wabern, ISBN 978-3-302-40077-8, 2018.

Berra, F., Galli, M. T., Reghellin, F., Torricelli, S., and Fantoni, R.: Stratigraphic evolution of the Triassic–Jurassic succession in the Western Southern Alps (Italy): the record of the two-stage rifting on the distal passive margin of Adria, Basin Res., 21, 335–353, https://doi.org/10.1111/j.1365-2117.2008.00384.x, 2009.

Berra, F., Tiepolo, M., Caironi, V., and Siletto, G. B.: U–Pb zircon geochronology of volcanic deposits from the Permian basin of the Orobic Alps (Southern Alps, Lombardy): chronostratigraphic and geological implications, Geol. Mag., 152, 429–443, https://doi.org/10.1017/S0016756814000405, 2015.

Berra, F., Felletti, F., and Tessarollo, A.: Stratigraphic Architecture of a Transtensional Continental Basin in Low-Latitude Semiarid Conditions: The Permian Succession of the Central Orobic Basin (Southern Alps, Italy), J. Sediment. Res., 86, 408–429, https://doi.org/10.2110/jsr.2016.26, 2016.

Bertotti, G., Picotti, V., Bernoulli, D., and Castellarin, A.: From rifting to drifting: tectonic evolution of the South-Alpine upper crust from the Triassic to the Early Cretaceous, Sediment. Geol., 86, 53–76, https://doi.org/10.1016/0037-0738(93)90133-P, 1993.

Bertotti, G., Seward, D., Wijbrans, J., Ter Voorde, M., and Hurford, A. J.: Crustal thermal regime prior to, during, and after rifting: A geochronological and modeling study of the Mesozoic South Alpine rifted margin, Tectonics, 18, 185–200, https://doi.org/10.1029/1998TC900028, 1999.

Bigi, G., Cosentino, D., Parotto, M., Sartori, R., and Scandone, P.: Structural Model of Italy Scale 1 V 500 : 000 – Consiglio 10 Nazionale delle Ricerche – Progetto Finalizzato Geodinamica, SELCA, Firenze, Italy, 1990.

Boehnke, P. and Harrison, T. M.: A meta-analysis of geochronologically relevant half-lives: what's the best decay constant?, Int. Geol. Rev., 56, 905–914, https://doi.org/10.1080/00206814.2014.908420, 2014.

Bonin, B., Brandlein, P., Bussy, F., Desmons, J., Eggenberger, U., Finger, F., Graf, K., Marro, C., Mercolli, I., Oberhänsli, R., Ploquin, A., Quadt von, A., Raumer von, J., Schaltegger, U., Steyrer, H.P., Visonà, D., and Vivier, G.: Late Varisican Magmatic Evolution of the Alpine Basement, in: The pre-Mesozoic Geology in the Alps, edited by: von Raumer, J., and Neubauer, F., Springer, Berlin, Germany, 169–199, https://doi.org/10.1007/978-3-642-84640-3, 1993.

Boriani, A. and Villa, I. M.: Geochronology of regional metamorphism in the Ivrea-Verbano zone and Serie dei Laghi, Italian Alps, Schweiz. Miner. Petrog., 77, 381–401, 1997.

Boriani, A., Burlini, L., and Sacchi, R.: The Cossato-Mergozzo-Brissago Line and the Pogallo Line (Southern Alps, Northern Italy) and their relationships with the late-Hercynian magmatic and metamorphic events, Tectonophysics, 182, 91–102, https://doi.org/10.1016/0040-1951(90)90344-8, 1990.

Boriani, A., Sassi, F., and Sassi, R.: The basement complexes in Italy, with special regards to those exposed in the Alps: a review, Episodes, 26, 186–192, https://doi.org/10.18814/epiiugs/2003/v26i3/006, 2003.

Brack, P. and Rieber, H.: Towards a better definition of the Anisian/Ladinian boundary: New biostratigraphic data and correlations of boundary sections from the Southern Alps, Eclogae Geol. Helv., 86, 415–527, 1993.

Cadel, G.: Geology and uranium mineralization of the Collio Basin (central Southern Alps, Italy), Uranium, 2, 215–240, 1986.

Carraro, F. and Ferrara, G.: Alpine "Tonalite" at Miagliano, Biella (Zona Diorito-Kinzigitica). A preliminary note, Schweiz. Miner. Petrog., 48, 75–80, 1968.

Carslaw, H. and Jaeger, J.: Conduction of Heat in Solids, Clarendon Press, Oxford, United Kingdom, 510 pp., ISBN-10: 0198533683, 1959.

Casati, P.: Tettonismo e sedimentazione nel settore occidentale delle Alpi Meridionali durante il tardo Paleozoico, il Triassico e il Giurassico, Riv. Ital. Paleontologia Stratigrafia, 84, 313–326, 1978.

Cassinis, G., Perotti, C. R., and Ronchi, A.: Permian continental basins in the Southern Alps (Italy) and perimediterranean correlations, Int. J. Earth Sci., 101, 129–157, https://doi.org/10.1007/s00531-011-0642-6, 2012.

Cassinis, G., Perotti, C., and Santi, G.: Post-Variscan Verrucano-like deposits in Italy, and the onset of the alpine tectono-sedimentary cycle, Earth-Sci. Rev., 185, 476–497, 2018.

Castellarin, A., Lucchini, F., Rossi, P. L., Selli, L., and Simboli, G.: The Middle Triassic magmatic-tectonic arc development in the Southern Alps, Tectonophysics, 146, 79–89, 1988.

Colombo, M., Di Capua, A., Livio, F., Scaramuzzo, E., and Tringali, G.: Volcanic and tectonic interaction during the Permian geodynamic event: new insights from the Lugano-Varese district, Southern Alps, (Italy-Switzerland), EGU General Assembly 2025, Vienna, Austria, 27 Apr–2 May 2025, EGU25-16466, https://doi.org/10.5194/egusphere-egu25-16466, 2025.

De Min, A., Velicogna, M., Ziberna, L., Chiaradia, M., Alberti, A., and Marzoli, A.: Triassic magmatism in the European Southern Alps as an early phase of Pangea break-up, Geol. Mag., 157, 1800–1822, https://doi.org/10.1017/S0016756820000084, 2020.

Di Battistini, G., Bargossi, G. M., Spotti, G., and Toscani, L.: Andesites of the late Hercynian volcanic sequence in Trentino Alto Adige (Northen Italy), Rendiconti Società Italiana Mineralogia Petrologia, 43, 1087–1100, 1988.

Diella, V., Spalla, M. I., and Tunesi, A.: Contrasting thermomechanical evolutions in the Southalpine metamorphic basement of the Orobic Alps (Central Alps, Italy), J. Metamorph. Geol., 10, 203–219, https://doi.org/10.1111/j.1525-1314.1992.tb00079.x, 1992.

Di Paola, S., Spalla, M. I., and Gosso, G.: New structural mapping and metamorphic evolution of the Domaso Cortafo Zone (Southern Alps-Lake Como), Memorie di Scienze Geologiche, Padova, 53, 1–14, 2001.

Doglioni, C.: Geological remarks on the relationships between extension and convergent geodynamic settings, Tectonophysics, 252, 253–267, https://doi.org/10.1016/0040-1951(95)00087-9, 1995.

Ehlers, T. A., Willett, S. D., Armstrong, P. A., and Chapman, D. S.: Exhumation of the central Wasatch Mountains, Utah: 2. Thermokinematic model of exhumation, erosion, and thermochronometer interpretation, J. Geophys. Res.-Sol. Ea., 108, 2173, https://doi.org/10.1029/2001JB001723, 2003.

Elter, F. M., Gaggero, L., Mantovani, F., Pandeli, E., and Costamagna, L. G.: The Atlas-East Variscan-Elbe shear system and its role in the formation of the pull-apart Late Palaeozoic basins, Int. J. Earth Sci., 109, 739–760, https://doi.org/10.1007/s00531-020-01830-y, 2020.

Ferrando, S., Bernoulli, D., and Compagnoni, R.: The Canavese zone (internal Western Alps): a distal margin of Adria, Schweiz. Miner. Petrog., 84, 237–259, 2004.

Festa, A., Balestro, G., Borghi, A., De Caroli, S., and Succo, A., The role of structural inheritance in continental break-up and exhumation of Alpine Tethyan mantle (Canavese Zone, Western Alps), Geosci. Front., 11, 167–188, https://doi.org/10.1016/j.gsf.2018.11.007, 2020.

Finger, F. and Steyrer, H. P.: I-type granitoids as indicators of a late Paleozoic convergent ocean–continent margin along the southern flank of the central European Variscan orogen, Geology, 18, 1207–1210, 1990.

Finger, F. and Steyrer, H. P.: Comments and Replies on I-type granitoids as indicators of a late Paleozoic convergent ocean–continent margin along the southern flank of the central European Variscan orogen, Geology, 19, 1245–1248, 1991.

Furrer, H.: The Kalkschieferzone (Upper Meride Limestone; Ladinian) near Meride (Canton Ticino, Southern Switzerland) and the evolution of a Middle Triassic intraplatform basin, Eclogae Geol. Helv., 88, 827–852, 1995.

Gaetani, M.: From Permian to Cretaceous: Adria as pivotal between extensions and rotations of Tethys and Atlantic Oceans, Journal of the Virtual Explorer, 36, 3–46, https://doi.org/10.3809/jvirtex.2010.00235, 2010.

Gaetani, M., Gnaccolini, M., Jadoul, F., and Garzanti, E.: Multiorder sequence stratigraphy in the Triassic system of the western Southern Alps: Mesozoic and Cenozoic sequence stratigraphy of European basins, SEPM Special Publications, 60, 701–717, 1998.

Gautheron, C., Tassan-Got, L., Barbarand, J., and Pagel, M.: Effect of alpha-damage annealing on apatite (U–Th)/He thermochronology, Chem. Geol., 266, 157–170, https://doi.org/10.1016/j.chemgeo.2009.06.001, 2009.

Giger, M.: Geochronologische und petrographische Studien an Geröllen und Sedimenten der Gonfolite Lombarda Gruppe (Südschweiz und Norditalien) und ihr Vergleich mit dem alpinen Hinterland, PhD thesis, University of Bern, Bern, Switzerland, 227 pp., 1991.

Giorno, M., Barale, L., Bertok, C., Frenzel, M., Looser, N., Guillong, M., Bernasconi, S., and Martire, L.: Sulfide-associated hydrothermal dolomite and calcite reveal a shallow burial depth for Alpine-type Zn-(Pb) deposits, Geology, 50, 853–858, https://doi.org/10.1130/G49812.1, 2022.

Govi, M: Geologia del territorio compreso tra il Lago di Lugano e la Val Marchirolo, Studi e Ricerche della Divisione Geomineraria del CNR, 3, 160–217, 1960.

Gretter, N., Ronchi, A., Langone, A., and Perotti, C. R.: The transition between the two major Permian tectono-stratigraphic cycles in the central Southern Alps: results from facies analysis and U/Pb geochronology, Int. J. Earth Sci., 102, 1181–1202, https://doi.org/10.1007/s00531-013-0886-4, 2013.

Handy, M. R., Franz, L., Heller, F., Janott, B., and Zurbriggen, R.: Multistage accretion and exhumation of the continental crust (Ivrea crustal section, Italy and Switzerland), Tectonics, 18, 1154–1177, https://doi.org/10.1029/1999TC900034, 1999.

Heberer, B., Reverman, R. L., Fellin, M. G., Neubauer, F., Dunkl, I., Zattin, M., Seward, D., Genser, J., and Brack, P.: Postcollisional cooling history of the Eastern and Southern Alps and its linkage to Adria indentation, Int. J. Earth Sci., 106, 1557–1580, https://doi.org/10.1007/s00531-016-1367-3, 2016.

Hourigan, J. K., Reiners, P. W., and Brandon, M. T.: U–Th zonation-dependent alpha-ejection in (U–Th)/He chronometry, Geochim. Cosmochim. Ac., 69, 3349–3365, https://doi.org/10.1016/j.gca.2005.01.024, 2005.

Hunziker, J. C.: Rb–Sr and K–Ar age determination and the Alpine tectonic history of the Western Alps, Mem. Ist. Geol. Mineral. Univ. Padova, 31, 5–55, 1974.

Hurford, A. J.: Cooling and uplift patterns in the Lepontine Alps South Central Switzerland and an age of vertical movement on the Insubric fault line, Contrib. Mineral. Petr., 92, 413–427, 1986.

Jäger, E. and Faul, H.: Altersbestimmungen an einigen Schweizer Gesteinen und dem Granit von Baveno, Schweiz. Miner. Petrog., 40, 10–12, 1960.

Jongmans, W. J. and Ritter, E.: Die Karbonflora der Schweiz, Beiträge zur geologischen Karte der Schweiz, Kümmerly und Frey, 116 pp., 1960.

Kalin, O. and Trümpy, D.: Sedimentation und Palaotektonik in den westlichen Sudalpen: Zur triasisch-jurassischen Geschichte des Monte Nudo-Beckens, Eclogae Geol. Helv., 70, 295–350, 1960.

Karakas, O., Wotzlaw, J. F., Guillong, M., Ulmer, P., Brack, P., Economos, R., Bergantzm G. W., Sinigoi, S., and Bachmann, O.: The pace of crustal-scale magma accretion and differentiation beneath silicic caldera volcanoes, Geology, 47, 719–723, https://doi.org/10.1130/G46020.1, 2019.

Ketcham, R. A., Gautheron, C., and Tassan-Got, L.: Accounting for long alpha-particle stopping distances in (U–Th–Sm)/He geochronology: Refinement of the baseline case, Geochm. Cosmochim. Ac., 75, 7779–7791, https://doi.org/10.1016/j.gca.2011.10.011, 2011.

Locchi, S., Zanchetta, S., and Zanchi, A.: Evidence of Early Permian extension during the post-Variscan evolution of the central Southern Alps (N Italy), Int. J. Earth Sci., 111, 1717–1738, https://doi.org/10.1007/s00531-022-02220-2, 2022.

Lorenz, V. and Nicholls, I. A.: Plate and intraplate processes of Hercynian Europe during the Late Paleozoic, Tectonophysics, 107, 25–56, 1984.

Malavieille, J., Guihot, P., Costa, S., Lardeaux, J. M., and Gardien, V.: Collapse of the thickened Variscan crust in the French Massif Central: Mont Pilat extensional shear zone and St. Etienne Late Carboniferous basin, Tectonophysics, 177, 139–149, 1990.

Marocchi, M., Morelli, C., Mair, V., Klötzli, U., and Bargossi, G. M.: Evolution of Large Silicic Magma Systems: New U–Pb Zircon Data on the NW Permian Athesian Volcanic Group (Southern Alps, Italy), J. Geol., 116, 480–498, 2008.

Marrett, R. and Allmendinger, R. W.: Kinematic analysis of fault-slip data, J. Struct. Geol., 12, 973–986, 1990.

Martin, S., Bigazzi, G., Zattin, M., Viola, G., and Balestrieri, M. L.: Neogene kinematics of the Giudicarie fault (Central-Eastern Alps, Italy): new apatite fission-track data, Terra Nova, 10, 217–221, 1998.

Martin, S., Toffolo, L., Moroni, M., Montorfano, C., Secco, L., Agnini, C., Nimis, P., and Tumiati, S.: Siderite deposits in northern Italy: Early Permian to Early Triassic hydrothermalism in the Southern Alps, Lithos, 284–285, 276–295, https://doi.org/10.1016/j.lithos.2017.04.002, 2017.

McDowell, F. W.: Potassium-argon ages from the Ceneri zone, Southern Swiss Alps, Contrib. Mineral. Petr., 28, 165–182, 1970.

McDowell, F. W. and Schmid, R.: Potassium-argon ages from the Valle d'Ossola section of the Ivrea-Verbano zone (northern Italy), Schweiz. Miner. Petrog., 48, 205–210, 1968.

Mohn, G., Manatschal, G., Müntener, O., Beltrando, M., and Masini, E.: Unravelling the interaction between tectonic and sedimentary processes during lithospheric thinning in the Alpine Tethys margins, Int. J. Earth Sci., 99, 75–101, 2010.

Mohn, G., Manatschal, G., Masini, E., and Müntener, O.: Rift-related inheritance in orogens: a case study from the Austroalpine nappes in Central Alps (SE-Switzerland and N-Italy), Int. J. Earth Sci., 100, 937–961, 2011.

Mohn, G., Manatschal, G., Beltrando, M., Masini, E., and Kusznir, N.: Necking of continental crust in magma-poor rifted margins: Evidence from the fossil Alpine Tethys margins, Tectonics, 31, TC1012, https://doi.org/10.1029/2011TC002961, 2012.

Molli, G., Brogi, A., Caggianelli, A., Capezzuoli, E., Liotta, D., Spina, A., and Zibra, I. Late Palaeozoic tectonics in Central Mediterranean: a reappraisal, Swiss J. Geosci., 113, 23, https://doi.org/10.1186/s00015-020-00375-1. 2020.

Muttoni, G., Kent, D. V., Garzanti, E., Brack, P., Abrahamsen, N., and Gaetani, M.: Early Permian Pangea 'B'to Late Permian Pangea "A", Earth Planet. Sc. Lett., 215, 379–394, https://doi.org/10.1016/S0012-821X(03)00452-7, 2003.

Muttoni, G., Gaetani, M., Kent, D. V., Sciunnach, D., Angiolini, L., Berra, F., Garzanti, E., Mattei, M., and Zanchi, A.: Opening of the Neo-Tethys Ocean and the Pangea B to Pangea A transformation during the Permian, GeoArabia, 14, 17–48, https://doi.org/10.2113/geoarabia140417, 2009.

Naliboff, J. B., Buiter, S. J., Péron-Pinvidic, G., Osmundsen, P. T., and Tetreault, J.: Complex fault interaction controls continental rifting, Nat. Commun., 8, 1179, https://doi.org/10.1038/s41467-017-00904-x, 2017.

Peron-Pinvidic, G., Manatschal, G., and Osmundsen, P. T.: Structural comparison of archetypal Atlantic rifted margins: A review of observations and concepts, Mar. Petrol. Geol., 43, 21–47, https://doi.org/10.1016/j.marpetgeo.2013.02.002, 2013.

Pohl, F., Froitzheim, N., Obermüller, G., Tomaschek, F., Schröder, O., Nagel, T. J., Schiunnach, D., and Heuser, A.: Kinematics and age of syn-intrusive detachment faulting in the Southern Alps: Evidence for Early Permian crustal extension and implications for the Pangea A versus B Controversy, Tectonics, 37, 3668–3689, https://doi.org/10.1029/2018TC004974, 2018,

Pomella, H., Stipp, M., and Fügenschuh, B.: Thermochronological record of thrusting and strike-slip faulting along the Giudicarie fault system (Alps, Northern Italy), Tectonophysics, 579, 118–130, https://doi.org/10.1016/J.Tecto.2012.04.015, 2012.

QGIS Association: QGIS Geographic Information System, QGIS Association [code and data set], https://qgis.org/it/site/, last access: 3 April 2024.

Quick, J. E., Sinigoi, S., Peressini, G., Demarchi, G., Wooden, J. L., and Sbisà, A.: Magmatic plumbing of a large Permian caldera exposed to a depth of 25 km, Geology, 37, 603–606, 2009.

Real, C., Fassmer, K., Carosi, R., Froitzheim, N., Rubatto, D., Groppo, C., Münker. C., and Ferrando, S.: Carboniferous–Triassic tectonic and thermal evolution of the middle crust section of the Dervio–Olgiasca Zone (Southern Alps), J. Metamorph. Geol., 41, 685–718, https://doi.org/10.1111/jmg.12714, 2023.

Reiners, P. W. and Brandon, M. T.: Using thermochronology to understand orogenic erosion, Annu. Rev. Earth Pl. Sc., 34, 419–466, https://doi.org/10.1146/annurev.earth.34.031405.125202, 2006.

Reiners, P. W., Spell, T. L., Nicolescu, S., and Zanetti, K. A.: Zircon (U–Th)/He thermochronometry: He diffusion and comparisons with $^{40}$Ar/$^{39}$Ar dating, Geochim. Cosmochim. Ac., 68, 1857–1887, https://doi.org/10.1016/j.gca.2003.10.021, 2004.

Renesto, S. and Stockar, R.: First record of a coelacanth fish from the Middle Triassic Meride Limestone of Monte San Giorgio (Canton Ticino, Switzerland), Riv. Ital. Paleontol. S., 124, 639–653, 2018.

Reverman, R. L., Fellin, M. G., Herman, F., Willett, S. D., and Fitoussi, C.: Climatically versus tectonically forced erosion in the Alps: Thermochronometric constraints from the Adamello Complex, Southern Alps, Italy, Earth Planet. Sc. Lett., 339, 127–138, https://doi.org/10.1016/j.epsl.2012.04.051, 2012.

Roda, M., Regorda, A., Spalla, M. I., and Marotta, A. M.: What drives Alpine Tethys opening? Clues from the review of geological data and model predictions, Geol. J., 54, 2646–2664, https://doi.org/10.1002/gj.3316, 2019.

Rosenberg, C. L. and Kissling, E.: Three-dimensional insight into Central-Alpine collision: Lower-plate or upper-plate indentation?, Geology, 41, 1219–1222, https://doi.org/10.1130/G34584.1, 2013.

Scaramuzzo, E., Livio, F. A., Granado, P., Di Capua, A., and Bitonte, R.: Anatomy and kinematic evolution of an ancient passive margin involved into an orogenic wedge (Western Southern Alps, Varese area, Italy and Switzerland), Swiss J. Geosci., 115, 4, https://doi.org/10.1186/s00015-021-00404-7, 2022.

Schaltegger, U. and Brack, P.: Crustal-scale magmatic systems during intracontinental strike-slip tectonics: U, Pb and Hf isotopic constraints from Permian magmatic rocks of the Southern Alps, Int. J. Earth Sci., 96, 1131–1151, https://doi.org/10.1007/s00531-006-0165-8, 2007.

Shuster, D. L., Flowers, R. M., and Farley, K. A.: The influence of natural radiation damage on helium diffusion kinetics in apatite, Earth Planet. Sc. Lett., 249, 148–161, https://doi.org/10.1016/j.gca.2008.10.013, 2006.

Siegesmund, S., Layer, P., Dunkl, I., Vollbrecht, A., Steenken, A., Wemmer, K., and Ahrendt, H.: Exhumation and deformation history of the lower crustal section of the Valstrona di Omegna in the Ivrea Zone, southern Alps, Geological Society, London, Special Publications, 298, 45–68, https://doi.org/10.1144/SP298.3, 2008.

Siletto, G. B., Spalla, M. I., Tunesi, A., Lardeaux, J. M., and Colombo, A.: Pre-Alpine structural and metamorphic histories in the Orobic Southern Alps, Italy, in: Pre-Mesozoic geology in the Alps, edited by: Von Raumer, J. F. and Neubauer, F., Springer, Berlin, Germany, 585–598, ISBN-10: 3642846424, 1993.

Spalla, M. I., Diella, V., Pigazzini, N.., Siletto, G. B., and Gosso, G.: Significato tettonico della transizione Cld-And nelle metapeliti del Basamento Sudalpino (Alta Val Camonica), Rendiconti della Società Geologica Italiana, 2, 182–183, 2006.

Stampfli, G. M.: The Intra-Alpine terrain: a Paleotethyan remnant in the Alpine Variscides, Eclogae Geol. Helv., 89, 13–42, 1996.

Stampfli, G. M.: Tethyan oceans, in: Tectonics and Magmatism in Turkey and Surrounding Area, edited by: Bozkurt, E., Winchester, J. A., and Piper, J. D. A., Geological Society, London, Special Publications, 173, 1–23, ISBN 1-86239-064-9, 2000.

Stampfli, G. M. and Kozur, H. W.: Europe from the Variscan to the Alpine cycles, in: European Lithosphere Dynamics, edited by: Gee, D. G. and Stephenson, R. A., Geological Society, London, Memoirs, 32, 57–82, https://doi.org/10.1144/GSL.MEM.2006.032.01.04, 2006.

Stille, P. and Buletti, M.: Nd-Sr isotopic characteristics of the Lugano volcanic rocks and constraints on the continental crust formation in the South Alpine domain (N-Italy-Switzerland), Contrib. Mineral. Petr., 96, 140–150, 1987.

Stockar, R.: Facies, depositional environment, and palaeoecology of the Middle Triassic Cassina beds (Meride Limestone, Monte San Giorgio, Switzerland), Swiss J. Geosci., 103, 101–119, https://doi.org/10.1007/s00015-010-0008-2, 2010.

Stockar, R., Adatte, T., Baumgartner, P. O., and Föllmi, K. B.: Palaeoenvironmental significance of organic facies and stable isotope signatures: the Ladinian San Giorgio Dolomite and Meride Limestone of Monte San Giorgio (Switzerland, WHL UNESCO), Sedimentology, 60, 239–269, https://doi.org/10.1111/sed.12021, 2013.

Storck, J. C., Brack, P., Wotzlaw, J. F., and Ulmer, P.: Timing and evolution of Middle Triassic magmatism in the Southern Alps (northern Italy), J. Geol. Soc. London, 176, 253–268, 2019.

Torsvik, T. H. and Cocks, L. R. M.: Earth geography from 400 to 250 Ma: a palaeomagnetic, faunal and facies review, J. Geol. Soc. London, 161, 555–572, 2004.

Visonà, D.: Plutonismo basico ercinico nel Sudalpino delle Alpi Orientali: primi dati per un modello di tettonica a placche ercinica, Rendiconti della Società geologica italiana, 5, 105–107, https://doi.org/10.1007/s005310100200, 1982.

Von Raumer, J., Stampfli, G., Borel, G., and Bussy, F.: Organization of pre-Variscan basement areas at the north-Gondwanan margin, Int. J. Earth Sci., 91, 35–52, 2002.

Welch, B. L.: The generalization of "Student's" problem when several different population variances are involved, Biometrika, 34, 28–35, 1947.

Willett, S. D., Herman, F., Fox, M., Stalder, N., Ehlers, T. A., Jiao, R., and Yang, R.: Bias and error in modelling thermochronometric data: resolving a potential increase in Plio-Pleistocene erosion rate, Earth Surf. Dynam., 9, 1153–1221, https://doi.org/10.5194/esurf-9-1153-2021, 2021.

Wilson, J. T.: Static or mobile earth: the current scientific revolution, P. Am. Philos. Soc., 112, 309–320, 1968.

Wilson, R. W., Houseman, G. A., Buiter, S. J. H., McCaffrey, K. J., and Doré, A. G.: Fifty years of the Wilson Cycle concept in plate tectonics: an overview, Geological Society, London, Special Publications, 470, 1–17, https://doi.org/10.1144/SP470-2019-58, 2019.

Winterer, E. L. and Bosellini, A.: Subsidence and sedimentation on Jurassic passive continental margin, Southern Alps, Italy, AAPG Bull., 65, 394–421, https://doi.org/10.1306/2F9197E2-16CE-11D7-8645000102C1865D, 1981.

Withjack, M. O., Islam, Q. T., and La Pointe, P. R.: Normal faults and their hanging-wall deformation: an experimental study, AAPG Bull., 79, 1–17, https://doi.org/10.1306/8D2B1494-171E-11D7-8645000102C1865D, 1995.

Wolff, R., Dunkl, I., Kiesselbach, G., Wemmer, K., and Siegesmund, S.: Thermochronological constraints on the multiphase exhumation history of the Ivrea-Verbano Zone of the Southern Alps, Tectonophysics, 579, 104–117, https://doi.org/10.1016/j.tecto.2012.03.019, 2012.

Zanchetta, S., D'Adda, P., Zanchi, A., Barberini, V., and Villa, I. M.: Cretaceous-Eocene compression in the central Southern Alps (N Italy) inferred from $^{40}Ar/^{39}Ar$ dating of pseudotachylytes along regional thrust faults, J. Geodyn., 51, 245–263, https://doi.org/10.1016/j.jog.2010.09.004, 2011.

Zanchetta, S., Malusà, M. G., and Zanchi, A.: Precollisional development and Cenozoic evolution of the Southalpine retrobelt (European Alps), Lithosphere, 7, 662–681, https://doi.org/10.1130/L466.1, 2015.

Zanchi, A., Zanchetta, S., Berio, L., Berra, F., and Felletti, F.: Low-angle normal faults record Early Permian extensional tectonics in the Orobic Basin (Southern Alps, N Italy), Ital. J. Geosci., 138, 184–201, https://doi.org/10.3301/IJG.2018.35, 2019.

Zanetti, A., Mazzucchelli, M., Sinigoi, S., Giovanardi, T., Peressini, G., and Fanning, M.: SHRIMP U–Pb zircon Triassic intrusion age of the Finero mafic complex (Ivrea–Verbano Zone, Western Alps) and its geodynamic implications, J. Petrol., 54, 2235–2265, 2013.

Zanoni, D. and Spalla, M. I.: The Variscan evolution in the basement cobbles of the Permian Ponteranica Formation by microstructural and petrologic analysis, Ital. J. Geosci., 137, 254–271, https://doi.org/10.3301/IJG.2018.12, 2018.

Zattin, M., Cuman, A., Fantoni, R., Martin, S., Scotti, P., and Stefani, C.: From Middle Jurassic heating to Neogene cooling: The thermochronological evolution of the southern Alps, Tectonophysics, 414, 191–202, https://doi.org/10.1016/J.Tecto.2005.10.020, 2006.

Ziegler, P. A. and Stampfli, G. M.: Late Paleozoic-Early Mesozoic plate boundary reorganization: collapse of the Variscan orogen and opening of Neotethys, in: Permian continental deposits of Europe and other areas. Regional reports and correlations, edited by: Cassinis, G., Monografie di Natura Bresciana, Grafo, Brescia, Italy, 17–34, 2001.

Zingg, A., Handy, M. R., Hunziker, J. C., and Schmid, S. M.: Tectonometamorphic history of the Ivrea Zone and its relationship to the crustal evolution of the Southern Alps, Tectonophysics, 182, 169–192, https://doi.org/10.1016/0040-1951(90)90349-D, 1990.

Zorn, H.: Paläontologische, stratigraphische und sedimentologische Untersuchungen des Salvatoredolomits (Mitteltrias) der Tessiner Kalkalpen: unter besonderer Berücksichtigung der Mikrofazies, Diagenese und Taxionomie der Lamellibranchiata, Schweiz. Paläontol. Abh., 91, 1–90, 1971.

Zwingmann, H. and Mancktelow, N.: Timing of Alpine fault gouges, Earth Planet. Sc. Lett., 223, 415–425, https://doi.org/10.1016/j.epsl.2004.04.041, 2004.